Electrochemical sensing directly in bodily fluids – a move towards point of care and *in vivo* analysis

by

Ruben Tomás

Dissertation submitted in partial fulfilment for the Degree of

Master of Science in Molecular Analytical Sciences

Supervisors: Dr Tony Bristow and Prof. Julie Macpherson

WARWICK

THE UNIVERSITY OF WARWICK

September, 2017

Table of Contents

Summary

In vivo sensing has become a fundamental topic in modern medicine due to the ability to directly interrogate biological processes in living organisms. However, few sensors meet the necessary criteria of an *in vivo* sensor, which must achieve good sensitivity, dynamic range, reversibility, biocompatibility and resistance to fouling. Currently, the focus of most *in vivo* sensors remains on monitoring normal biological function, whereas there is also need to study pharmaceutical compounds, such as acetaminophen (APAP), for therapeutic monitoring and understanding toxicological effects. Herein, we proposed the use of boron-doped diamond (BDD), as a material for *in vivo* sensing of APAP. The effects of sp^2 carbon on the ability to probe biological matrices were also investigated using electrodes containing varying sp^2 content focusing on specificity and detection limits.

Proof-of-concept was ascertained through *in vitro* work by analysing APAP in the presence of 4% bovine serum albumin and synthetic urine, using cyclic voltammetry and differential pulse voltammetry (DPV). Electrodes containing greater sp^2 content exhibited increased fouling in the presence of albumin attributed to the adsorption of hydrophilic domains onto the electrode surface. However, sp^2 content was not the sole contributor to electrodes performance, but also the manner of electrode fabrication, treatment and material growth. Despite this, all electrodes demonstrated sufficient limits of detection (LOD) and quantification (LOQ) for monitoring therapeutic APAP concentrations in blood. Electrodes containing minimal sp^2 content achieved superior reproducibility, linearity, LOD (0.428 µM) and LOQ (1.30 µM). However, by varying sp^2 content, the oxidation potential of APAP shifted and thus can be used to increase specificity.

Unmodified BBD was not only uncovered as a prospective material for *in vivo* measurements of APAP in blood, but also for the rapid detection of minute concentrations present in urine. BDD demonstrated LOD (0.0487 µM) and LOQ (0.148 µM) capabilities sufficient to measure APAP concentrations in urine after oral administration of therapeutic doses, in the presence of caffeine. Furthermore, two adjacent oxidation peaks were observed for APAP in synthetic urine using BDD electrodes, improving the ability to identify APAP conclusively. DPV revealed the ability to increase the separation between these adjacent peaks by simply changing two parameters, demonstrating exceptional selectivity and sensitivity. Furthermore, simultaneous detection of caffeine, uric acid and APAP in synthetic urine further demonstrated the specificity of BDD electrodes.

This work has paved the way for future *in vivo* research using BDD which, if successful, could revolutionise personalised medicine by ensuring that the correct drug is provided at the right time and dose.

Acknowledgments

Abbreviations

A - electrode surface area (cm^2)

AA - ascorbic acid

APAP - acetaminophen (or N-acetyl-p-aminophenol)

BDD - boron-doped diamond (BDD)

BSA - bovine serum albumin

C - capacitance

c* - bulk concentration ($mol cm^{-3}$)

CAFF - Caffeine

CV - cyclic voltammetry

D - diffusion coefficient ($cm^2 s^{-1}$)

DPV - differential pulse voltammetry

E - applied electrode potential

E^o - standard electrode potential

ET - electron transfer

F - Faraday's constant (96485 C mol^{-1})

GC - glassy carbon

GCE - glassy carbon electrode

HSA - human serum albumin

I - faradaic current

i_{pa} - anodic peak current

i_{pc} – cathodic peak current

j - flux, or the rate of reaction (mol cm^{-2} s^{-1}).

LOD - limit of detection

LOQ - limit of quantification

MWCNTs/GCE - multi-walled carbon nanotubes film coated glassy carbon electrode

n - number of electron transferred

NAPQI - N-acetyl-p-benzoquinone-imine

NDC - non-diamond carbon

ORR - oxygen reduction reactions

PAPS - 3'-Phosphoadenosine-5'-phosphosulfate

Q - charge passed

SCE - saturated calomel electrode

SNR - signal-to-noise ratio

SW - solvent window

SWCNT-CCE - single-walled carbon nanotube-modified carbon-ceramic electrode

SWV - square-wave voltammetry

UA - uric acid

UDP - uridine 5'-diphospho

UGT - glucuronosyltransferase

v - scan rate (V s^{-1})

Γ - quinone surface coverage (mol cm^{-2}).

ΔE_P - potential peak difference

η - overpotential

List of Figures

List of Tables

Word Count

This document consists of 8797 words (excluding all titles, tables, figures, summary, references etc.).

1.   Introduction

Electroanalysis is defined as the application of electrochemistry, the branch of physical chemistry concerned with the interaction of electrical energy and chemical change, to elucidate analytical problems.[1,2] The increasing importance and prevalence of electrochemistry as an area of research for analytical applications is due to its relatively low cost, specificity, selectivity, low detection limits, ability to obtain results in real time, simplicity, rapid analysis time, ability to be miniaturised and applicability for *in situ* analysis.[3] Such advantages have led to the development of electrochemical devices suitable for; environmental studies (pollution monitoring,[4,5] environmental protection and non-polluting energy sources);[6] healthcare diagnostics;[7–10] microbial electrochemistry studies[11]; and, most importantly for this study, *in vivo* sensing.[12–14]

1.1   In Vivo Sensing

In vivo sensing has become a fundamental topic in modern medicine due to the ability to directly interrogate biological processes in living organisms.[15] Such sensors enable a better understanding and continuous monitoring of aberrations in normal biological functions, facilitating the ability to provide rapid diagnostics and treatments. Furthermore, personalised medicine is capable of revolutionising medicine by allowing the correct drug to be delivered at the right time and dose.[16] Consequently, from the realisation of this potential, a surge in recent advancements in the development of biosensors capable of detecting small molecules, protein targets and nucleic acids have been witnessed.[17,18]

The first *in vivo* sensors capable of real-time analysis were electrochemical glucose detectors that exploited the catalytic activity of glucose oxidase for the simple and reliable detection of glucose levels over time.[19] Additional platforms exist for continuous, real-time measurements (e.g. for lactate, nitrogen species and oxygen),[20] however, the biological recognition element, which provides quantitative or semi-quantitative information, is highly specific making it complex, expensive to synthesise and prevents the monitoring of other analytes.[21] Furthermore, few sensors meet the necessary criteria of an *in vivo* sensor, which must achieve sufficient sensitivity, dynamic range, reversibility, biocompatibility (biologically inert, whilst also leaving normal biology unperturbed) and resistance to fouling.[22]

Since then, development of microfluidic electrochemical detectors for *in vivo* continuous monitoring (MEDIC) has allowed the continuous tracking of numerous circulating drugs in living subjects, including doxorubicin (a chemotherapeutic) and kanamycin (an antibiotic) achieving high specificity and sensitivity at sub-minute temporal resolution.[23] MEDIC utilises an electrochemical aptamer-based sensor, consisting of a conformation-changing aptamer probe which, upon binding to a target molecule, undergoes conformational arrangement. This change modulates a redox current, generating an electrochemical signal. Due to the specificity of the device, reconfiguration is required to

measure further analytes by exchanging probes for one's specific to the analyte of interest. Thus, this requires that suitable probes exist and, if not, can be costly to produce. Furthermore, it is unknown whether these probes are suitable for long-term measurements and monitoring doses of common analgesic drugs.

Herein, we propose the use of unmodified boron-doped diamond (BDD) as a potential material for the development of novel *in vivo* sensors. Such a sensor would lack the extreme specificity of biosensors, due to the absence of biorecognition elements (e.g. an enzyme), potentially allowing the simultaneous detection of multiple analytes. However, the ability to distinguish between components in complex biological matrices is still required and was explored in this study.

1.2   Polycrystalline Boron-Doped Diamond

1.2.1   Properties of Boron-Doped Diamond

BDD has recently emerged as a prevalent material in electrochemistry due to the advantageous and extreme properties of diamond's complete sp^3 hybridisation of carbon, resulting in extensive tetrahedral bonding throughout the lattice, and the modified electrical properties provided by boron (p-type dopant).[24] Such properties, which surpass those of conventional electrode materials, include low capacitance (C), resistance to fouling, high chemical inertness, extended solvent window (SW), high thermal conductivity, mechanical robustness and biocompatibility.[25]

The unique properties of BDD suggest that the material is most suited for *in vivo* applications in comparison to gold, platinum and glassy carbon (GC). Capacitive current, also referred to as "non-faradaic" current, is the intrinsic background charge formed due to the accumulation of electrical charge on the electrode surface and in the electrolyte solution near the electrode (double layer), not due to charge transfer processes. Therefore, a lower capacitance is desired when measuring small currents and to ensure that all measurements represent the faradaic (electron transfer) process. This is especially important when monitoring small concentrations within biological systems. Resistance to fouling and mechanical robustness is required to ensure that even after prolonged exposure to complex biological matrices the electrode remains stable with high signal-to-noise ratios (SNR).[23] High chemical inertness prevents signals of interest from being masked by interferences (i.e. from oxygen and organic chemicals).[25] Finally, the extended SW allows the application of a large potential range without the oxidation and reduction of biological matrices, increasing the number of analytes that could be investigated.

Macpherson discusses that the properties of BDD can vary significantly from each electrode depending on diamond growth and treatment, which in turn affects surface morphology, boron dopant density, surface termination, non-diamond carbon (NDC) and surface finish.[24] Although BDD exhibits properties that demonstrate biological compatibility, and thus may be used as sensors in biological and medical experiments, achieving pure sp^3 material is often unattainable during diamond synthesis, especially in conjunction with high boron dopant levels and smaller-sized grain material.[26,27] Disadvantages associated with higher NDC (sp^2 containing diamond-π bonds) include: reduced SW, increased capacitance (and decreased LOD) and increased susceptibility to fouling.[28] However, the incorporation of sp^2 content can be beneficial, providing enhanced electrocatalytic properties and presence of surface bound quinone groups. Hence, it is important to assess sp^2 content for each application, to see how it impacts the measurement of interest.

Traditionally, Raman spectroscopy is used to determine the sp^2 content of diamond. Pure diamond possesses only sp^3 carbon (σ bonds) producing a single diamond zone centre optical phonon peak at 1332 cm^{-1}, whereas sp^2 carbon (π bonds) produces two peaks.[24] The first peak (at 1355 cm^{-1}) relates to the breathing mode of sp^2 rings, whilst the second peak (at ~1575 cm^{-1}) is a result of stretching of pairs of sp^2 sites (chains and rings). Comparing the ratio of the sp^3 and sp^2 peaks is the most widely used method to assess sp^2 content in BDD electrodes. However, this method is mainly qualitative and works best with electrodes of the same dopant density.[29] In addition, Raman penetrates several microns into the surface providing information over a depth range, rather than the more important surface content.[30]

In this study, sp^2 content was assessed by taking quinone surface coverage measurements of four electrodes, including a GC electrode (GCE); two BDD electrodes possessing sp^2 content that has been controllably introduced using laser ablation methods (GEN1 and GEN3); and an all-diamond device. This approach, proposed by Ayres *et al.*,[28] exploits the pH-dependent redox signature of activated surface bound quinone groups and linear relationship between quinone surface coverage and sp^2 content. Quinone oxidation peaks are integrated to obtain the charge passed, Q, and converted to quinone surface coverage (Γ) using equation 1.1.

$$Q = nAF\Gamma \tag{1.1}$$

where n = number of electron transferred; A = total electrode surface area (cm^2); and F = Faraday's constant (96485 C mol^{-1}). These measurements were subsequently used to investigate whether increased sp^2 coverage may be beneficial for *in vivo* measurements.

1.2.1 *Applications of BDD for In Vivo and In Vitro Sensing*

BDD's advantageous properties have been exploited in multiple *in vivo* and *in vitro* applications including measurements of norepinephrine released from the sympathetic nervous system of rat mesenteric arteries;[31] the measurement of neurotransmitters from single cells, such as adrenal chromaffin cells, and tissues;[32,33] detection of serotonin in the enterochromaffin cells of the intestinal mucosal layer in guinea pigs and rabbit ileum,[34–37] lymphocytes of adult rhesus monkeys,[38] and metacerebral cell of *Aplysia californica*;[39] and more.[40–43] Earlier *in vitro* and *in vivo* studies used carbon fibre electrode, however these studies were often hindered due to fouling, low SNR, instability, increased response variability, limit of detection (LOD) and linear dynamic range.[44] However, these studies highlight BDD's wide applicability in biological research.

Despite these recent advancements, minimal *in vitro* and *in vivo* studies using BDD for the quantitative analysis of some of the most commonly used pharmaceutical compounds exist. Currently, the focus of most *in vivo* sensors remains on monitoring normal biological function. Thus, as a preliminary study, acetaminophen (N-acetyl-p-aminophenol; APAP) was investigated in the presence of albumin, synthetic urine and various added compounds. *In vitro* data is fundamental for the development of *in vivo* sensors, so this research will provide the necessary basis for future work.

1.3 Pharmaceutical Compounds and Biological Matrices of Interest

1.3.1 *Acetaminophen, Caffeine and Ascorbic acid*

APAP, commonly referred to as paracetamol, is a widely used minor analgesic drug, possessing antipyretic and some cyclooxygenase inhibiting properties used to treat minor aches and pyrexia.[45] Patients who cannot tolerate aspirin, owing to the effects of salicylates on the gastric mucosa, often opt for APAP as an alternative.[46] Although administration of therapeutic dosages causes no side effects, APAP overdose can cause fulminating hepatic necrosis,[47] acute renal failure (rare),[48] acute pancreatitis,[49] and even death.[50] This is a great concern as APAP is one of the most frequently used drugs in intentional overdose due to its ease of access.[51] Thus, monitoring APAP concentration *in vivo*, as with most pharmaceutical compounds, is important for therapeutic monitoring and to study possible toxicological effects.

Fig. 1 summarises the pharmacokinetic pathway following the consumption of therapeutic doses of APAP. Once absorbed, therapeutic blood concentrations of APAP range from 5 to 20 mg L^{-1}.[52] Such LODs are attainable using electroanalytical methods of analysis. However, subsequent to absorption,

The therapeutic recommended oral dosage of acetaminophen for adults is one or two 500 mg tablets every 4 to 6 hours.

APAP is absorbed in the gastrointestinal tract by passive transport.[127] Absorption in the stomach is negligible but very rapid in the small intestine, approximately 30-60 min after administration of therapeutic doses.[128] However, the rate of absorption is dependent on gastric emptying.[129] The therapeutic The therapeutic blood concentration blood concentration ranges from 5 to 20 mg L^{-1}. [52,53,121]

APAP is rapidly and extensively metabolised at therapeutic concentrations with approximately 90% being metabolised in the liver *via* three metabolic pathways.[53,54]

At therapeutic dosages, APAP is excreted as sulphate conjugates (20-30%), glucuronide conjugates (45-55%), cysteine (15-55%) and unmodified acetaminophen (<5%).[121]

Figure 1. Pharmacokinetic pathway of APAP. Three notable metabolic pathways of APAP exist. Glucuronidation, which is responsible for ~45-55% of APAP metabolism, is catalysed by uridine 5'-diphospho (UDP)-glucuronosyltransferase (UGT).[121] UGT transfers the glucuronosyl group from UDP-flucuronic acid to make APAP more water-soluble. Sulfation (responsible for 20-30% of APAP metabolism) is catalysed by the cytosolic enzyme sulfotransferase.[53] This process makes APAP more polar and prone to elimination by transferring a sulfo group from 3'-Phosphoadenosine-5'-phosphosulfate (PAPS) to APAP. Finally, approximately 5-10% of APAP is oxidised by cytochrome P-450 to form highly reactive N-acetyl-*p*-benzoquinone-imine (NAPQI), which is detoxified by conjugation with glutathione and excreted in the urine as cysteine and mercapturic acid.[121] Hepatic necrosis is caused by a depletion in glutathione and build-up of NAPQI which covalently binds to the cysteine groups of cellular protein macromolecules in the liver.

metabolism occurs in the liver (~90%), gut and kidney, resulting in less than 5% of unmodified APAP in urine.[53,54] Hence, the LOD of BDD using two electrochemical experiments, cyclic voltammetry (CV) and differential pulse voltammetry (DPV), were subject to investigation to determine their feasibility

for *in vivo* applications. Furthermore, the linear dynamic range was also ascertained to determine if it is suitable for use in both therapeutic and overdose cases. Toxic blood concentrations range from 25-150 mg L^{-1} and the minimum lethal blood APAP concentration is considered 160 mg L^{-1}, whilst 300 mg L^{-1} is the mean lethal blood concentration.[52]

Various techniques have been utilised for APAP determination in pharmaceutical and medical applications including spectrophotometry,[55,56] spectrofluorimetry,[57,58] chemiluminescence,[59] Raman spectroscopy,[60] Fourier transform infrared spectrophotometry,[61] liquid chromatography[62,63], titrimetry[64,65] and capillary electrophoresis.[66] However, spectroscopic methods often suffer from interferences of other phenolic compounds, including 4-aminophenol (produced by paracetamol hydrolysis) and thus require sample pre-treatments (e.g. complex formation and extraction) which can be laborious and time-consuming.[67] Chromatographic techniques do not suffer from these issues but can require the use of expensive equipment and derivatisation reagents. Electroanalytical methods are popular due to their low cost, short time consumption, high selectivity and sensitivity and simplicity compared to the aforementioned methods. Furthermore, substances often coadministered with APAP interfere with other techniques but are not electroactive.[67]

Although this research's prime focus is the ability to detect APAP in biological fluids, it is also important to be able to detect the presence of, or be able to distinguish from, additional drugs often combined with APAP. Caffeine (1,3,7-trimethylxanthine) is the most widely consumed psychoactive drug due to its abundance in food and beverages. Furthermore, it can also be included in some analgesic preparations due to its diuretic action.[68] Thus, although the detection of caffeine has no significant clinical importance, the ability to distinguish between caffeine and paracetamol is crucial for this study. Moreover, ascorbic acid (AA) is also often present in pharmaceutical preparations and metabolic fluids due to the synergetic and protective effects provided when used in conjunction with APAP for therapeutic purposes.[69] APAP's favourable effects are intensified while reducing potential toxicity in the function of the liver.[70] Also, humans are unable to synthesise AA endogenously, making it an essential dietary component. Although analytical methods exist for the analysis of caffeine and AA individually,[71–73] minimal work has been conducted on the ability to identify paracetamol in the presence of these additional analytes and biological matrices.

Fig. 2 illustrates the proposed electrochemical oxidation mechanisms of APAP, AA and caffeine.[74–77] Benschoten *et al.* investigated the electrochemical oxidation of APAP through CV studies.[78] The first reaction is a two-electron oxidation process resulting in the loss of two protons, which generates NAPQI. At pH values above 6, NAPQI exists in its stable unprotonated form (Fig. 2). Any subsequent follow-up chemical reactions are pH-dependent. The electroactive properties of APAP have been widely exploited, for the quantitative analysis of pharmaceutical formations. Various

(a)   Acetaminophen

(b)   Ascorbic acid
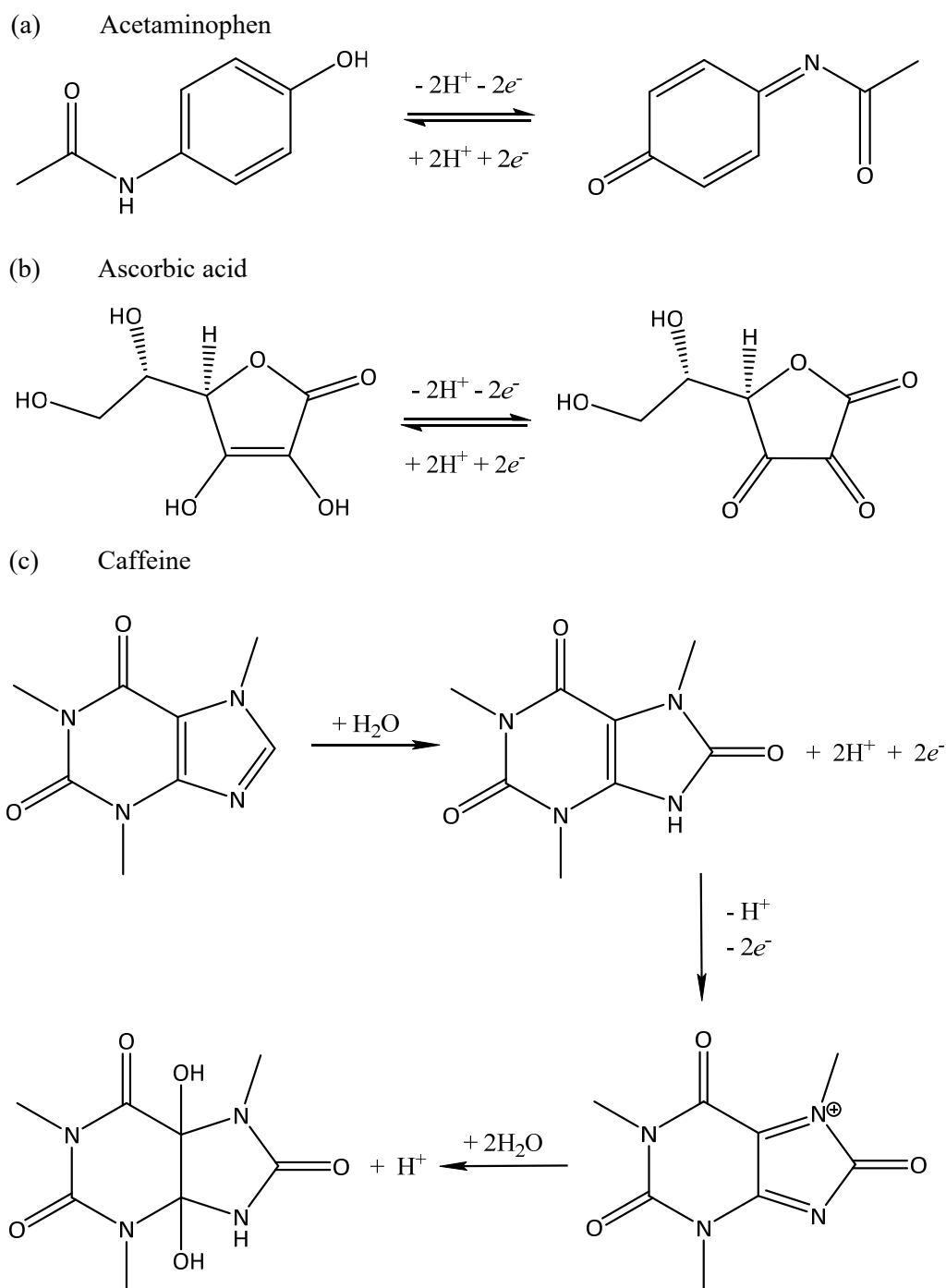
(c)   Caffeine

Figure 2. Oxidation mechanisms of APAP, AA and caffeine. Oxidation of APAP is a two-electron oxidation process, generating unprotonated NAPQI at pH values above 6. AA, as an enol hexose acid lactone, is easily oxidised electrochemically to L-dehydroascorbic acid *via* the hydrogens from the enol type hydroxyls, which subsequently undergoes irreversible hydration to 2,3-diketo-L-gulonic acid.[74] Hansen and Dryhurst and Spătaru proposed the above four-electron, four-proton oxidation mechanism of caffeine oxidation which is also hydrated to an electroinactive species.[75–77]

materials have been studied including GCE,[79] multi-walled carbon nanotubes film coated glassy carbon electrode (MWCNTs/GCE),[80] modified graphene oxide electrodes (Al$_2$O$_3$-Au/PDDA/rGO/GCE)[81] and cathodically pre-treated BBD electrode.[82] These studies demonstrate the excellent dynamic range

capable of these materials, minimal interference of APAP detection in the presence of additional pharmaceutically active compounds, and sufficient LOD for *in vivo* applications. Furthermore, the simultaneous detection of APAP and AA has also been achieved using unmodified BDD,[83] BBD modified with Nafion and lead films[84] and a GCE.[85]

Although these studies show great promise for the analysis of pharmaceutical formulations, the results obtained are not directly relatable to the analysis of biological matrices. Firstly, the electrodes modified would not all be applicable for *in vivo* purposes as care must be taken to ensure that functionalisation is complete with materials that are non-toxic, that will not unbind to the surface and possess long-term stability in harsh conditions. In addition, although assessment of possible interferences of additional pharmaceutical compounds was conducted, the complex nature of biological matrices possesses further potential interfering compounds. Finally, the supporting electrolytes utilised are often expensive and have been selected to provide optimum peak separation, peak current and shape which cannot be selected when conducting *in vivo* analysis. The majority of the work was carried out using acidic buffers (pH between 2 – 5) to provide optimum results, whereas the pH of bodily fluids can range from 4.6 to 8.[86] The pH value is of importance as the peak potential of APAP is pH-dependent, due to the involvement of protons in the oxidation reaction. As the pH of the supporting electrolyte increases, the peak potential shifts towards less positive values, there is an increase in peak half-width and peak current begins to decrease.[80,87,88] Navarro *et al.* provides three reasons for this: firstly, the heterogenous rate constant (affected by proton transfer) decreases with increasing pH; secondly, the homogenous rate constant is expected to affect pulse curves, as it increases with increasing pH; and finally, the increased acid-base catalysed hydrolysis of APAP at higher pH's leads to the formation of reducing compounds such as 4-aminophenol.[87]

Recently, various materials have been used for the simultaneous detection of APAP and additional analytes in biological fluids. Such materials include: MWCNTs/GCE,[89] carbon paste electrode,[87] cathodically pre-treated BDD,[90] single-walled carbon nanotube-modified carbon-ceramic electrode (SWCNT-CCE),[69] MWCNTs:graphite/GCE,[91] and a single walled carbon nanotube/chitosan/room temperature ionic liquid nanocomposite modified GCE.[92] These studies utilise materials with the potential for miniaturisation and of low cost whilst still providing results of good accuracy, precision, large linear dynamic range and sufficient LOD and limit of quantification (LOQ) for *in vivo* applications. Although carbon nanotubes enhance LODs by increasing electrode surface area, biocompatibility remains an issue. Carbon nanotubes are believed to be toxic and exposure can influence *in vivo* behaviour.[93] Furthermore, the difficulty of growing carbon nanotubes poses reproducibility issues.[94] We believe that unmodified BDD would be suitable for *in vivo* sensing without the need for surface modification, whilst achieving comparable results and retaining biocompatibility.

1.3.2   Human Serum Albumin and Synthetic Urine

To assess whether BDD is suitable for measurements in biological matrices, such as blood and urine, preliminary studies were carried out using a 4% bovine serum albumin (BSA) solution, in pH 7.4 phosphate buffered saline (PBS), and synthetic urine.

Human serum albumin (HSA) is the most abundant protein in the blood plasma (52% of total protein composition), possessing multiple physiological functions attributed to the unique single-polypeptide multidomain globular structure. The most important functions include: serving as a protein storage and transport component for both exogenous and endogenous compounds, maintenance of normal colloid osmotic pressure, metabolic functions, and anticoagulant effects.[95–97] Previous studies have shown that APAP binds to HSA (binding ratio of 2:1, respectively) through hydrogen bonding and hydrophobic interactions mainly through the binding site located in the hydrophobic pocket of subdomain IIIA.[98] Thus, APAP detection in a 4% albumin solution was completed as a preliminary study to determine its feasibility for the analysis of APAP in blood.

Analysis of APAP in synthetic urine was also completed for a similar purpose. Although the exact contents of synthetic urine were unknown, it possesses the major components of human urine within accepted ranges (urea, creatinine, inorganic salts, etc.).[99] Synthetic urine and 4% BSA solutions were used to test for electrode fouling, capacitance and SW and the LOD, LOQ and linear dynamic range of APAP. Furthermore, the use of synthetic urine provides an indication of any potential interfering compounds present in human urine.

1.4   Aims and objectives

To summarise, this preliminary study aims to determine if BDD is a suitable material for *in vivo* electrochemical measurements of APAP and to investigate if added sp^2 content is beneficial for such measurements. The following objectives were set in the hopes to answer these questions:

- Obtain quinone surface coverage measurements of an all-diamond electrode, two laser ablated diamond electrodes (GEN1 and GEN3) and a GC electrode to determine sp^2 content.
- Carry out capacitance, SW and fouling measurements of electrodes in PBS, 4% BSA and synthetic urine to ensure normal functioning of electrodes even in biological matrices.
- Ascertain the dynamic linear range, LOD and LOQ of APAP in 4% BSA and synthetic urine to determine if feasible for future *in vivo* work.
- Distinguishing AA, APAP and caffeine in synthetic urine to study the specificity of all electrodes.

1.5 Electrochemistry Background

1.5.1 Dynamic electrochemistry

Dynamic electrochemistry, which forms the basis of experiments carried out in this study, induces a chemical reaction through the application of a potential resulting in a specific electron transfer (ET) process with a chemical species at the electrode interface and electrolyte solution.[100] ET produces a measurable current which, when measured as a function of the applied potential, provides information relating to the process occurring at the electrode/electrolyte interface. This forms the basis of voltammetry experiments.

To explain this further, a simple electrochemical reaction is expressed by equation 1.1:

$$O + n\text{e-} \rightleftharpoons R \tag{1.1}$$

where R and O denote the reduced and oxidised form of an electroactive species, respectively. The position of the equilibrium can be perturbed to drive either a reduction or oxidation reaction at the electrode/electrolyte interface. This is accomplished by applying an overpotential ($\eta = E - E^{o}$), where the applied electrode potential (E) is either greater (oxidation) or less (reduction) than the standard electrode potential for the electroactive species (E^{o}). Fig. 3 illustrates how this is possible.

ET results in the flow of current (i) which, as predicted by the Butler-Volmer model, increases exponentially with increasing η. Current is also dependent on various other factors, as illustrated in equation 1.2.

$$i = nAFj \tag{1.2}$$

Where I = the faradaic current; n = number of electron transferred; F = Faraday's constant (96485 C mol^{-1}); A = the electrode surface area (cm^{2}); and j = flux, or the rate of reaction (mol cm^{-2} s^{-1}). Fig. 4 illustrates the typical electrode pathway required to achieve reduction, or oxidation.
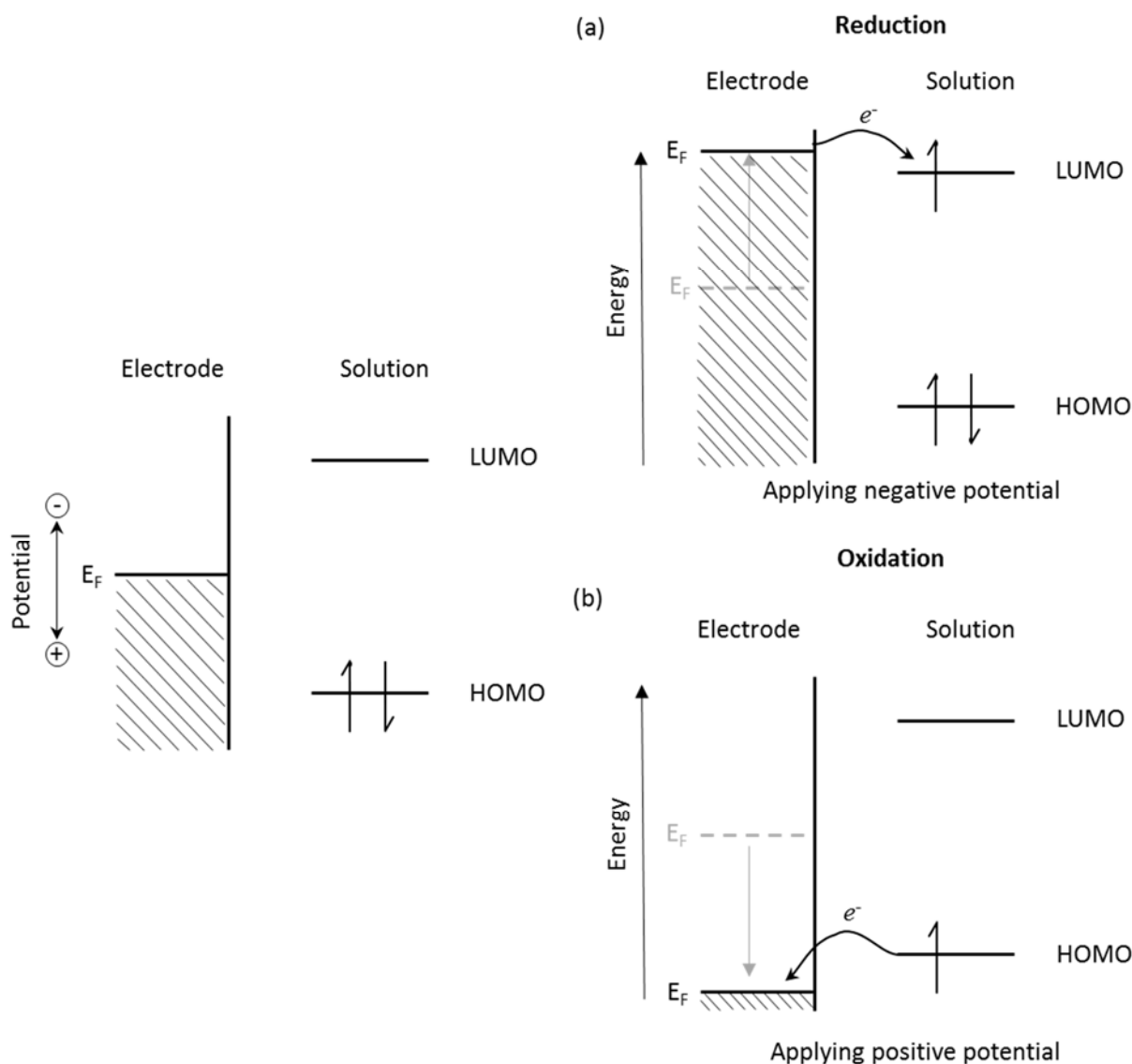
Figure 3. Schematic of (a) reduction and (b) oxidation process of species in dynamic electrochemistry. An electrical potential applied to a metal acts to increase or decrease the Fermi energy level, the maximum energy level in which electrons occupy an effective continuum of energy states in a metal.[101] A negative potential increases the Fermi energy level. Once sufficiently negative, the species is reduced. Application of a positive potential results in a decrease in the Fermi energy level of the metal, so oxidation becomes more thermodynamically favourable. Thus, application of different potentials can be used to drive specific ET processes, despite being thermodynamically unstable.
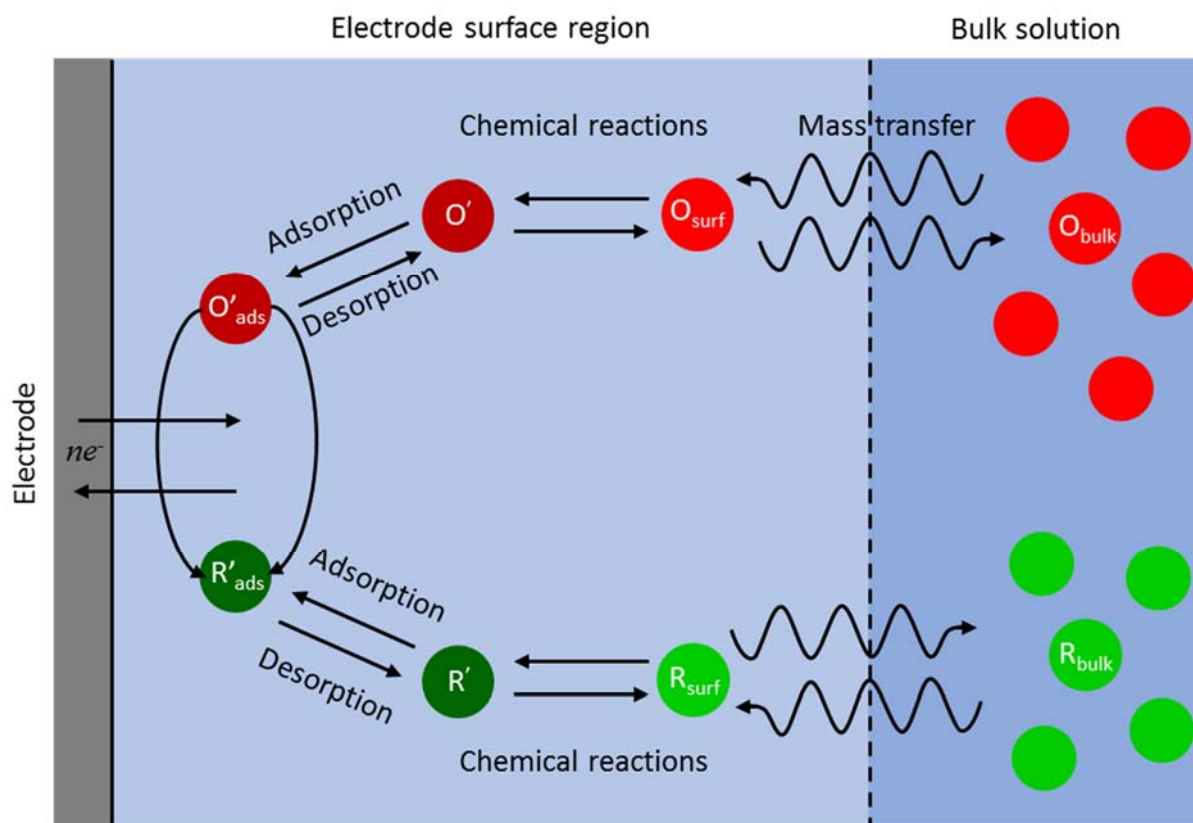
Figure 4. General electrode reaction pathway. In order to achieve reduction, or oxidation, a typical electrode pathway is: (1) mass transport of the electroactive species from the bulk solution (O_{bulk}) to the electrode surface region; (2) chemical reactions, including homogeneous (e.g. dimerization or protonation) and heterogeneous processes (e.g. catalytic decomposition); (3) surface reactions, whereby adsorption or desorption of the chemical species takes place and (4) ET at the electrode surface.[100] The rate of the reaction, or flux (j), is controlled by either mass transport or ET depending on which is the slowest step.

Mass transport occurs *via* three main processes; convection, migration and diffusion.[102] Convection, the movement of fluid due to natural (temperature and pressure gradients) or forced convection (stirring, rotating and vibrating), is often used to enhance the rate of mass transport. Convection is neglected if no stirring is used and constant temperature and pressure are maintained. Migration is the movement of charged particles down a potential gradient due to the electric field always present in electrochemical systems. Migration can diminish (in the case of reduction of anions), or enhance (during the reduction of cations) the current flowing to the electrode. The addition of a high ionic strength background electrolyte screens the electrode surface shielding the bulk solution from the electric field. Diffusion is the movement of electroactive species due to the formation of a concentration gradient and is always present. Thus, diffusion must always be considered when acquiring electrochemical measurements.

ET can occur by inner or outer sphere processes. For an outer sphere ET, the electron is transferred from the working electrode to the mediator forming either a ligand-centred ion or metal-centred ion. Following this, the electron travels to the substrate through space. The other method, which is less

entropically favourable, is inner sphere ET where the electron is transferred *via* a covalent linkage between a ligand-centred ion and the substrate. Thus, inner sphere processes are dependent on surface chemistry and electrode material.

1.5.2 Experimental Setup

A three-electrode setup immersed in an electrolyte solution, as illustrated in Fig. 5, was used throughout this study. ET processes take place at the working electrode. A potentiostat applies a potential between the working and reference electrode and measures current between the working and counter electrode. The reference electrode has a stable and well-defined electrode potential, which is usually used as a half cell to build an electrochemical cell. This provides a fixed point from which a potential difference is applied to the working electrode. A saturated calomel electrode (SCE) was used for all experiments. Finally, the counter electrode consists of a high surface area conductor that is inert (e.g. gauze or Pt wire). A counter electrode is necessary when using macro electrode (radius ≥ 1 mm) due to the measurement of large currents ($>\mu$A) resulting in Ohmic drop, a loss in potential from solution resistance effects.
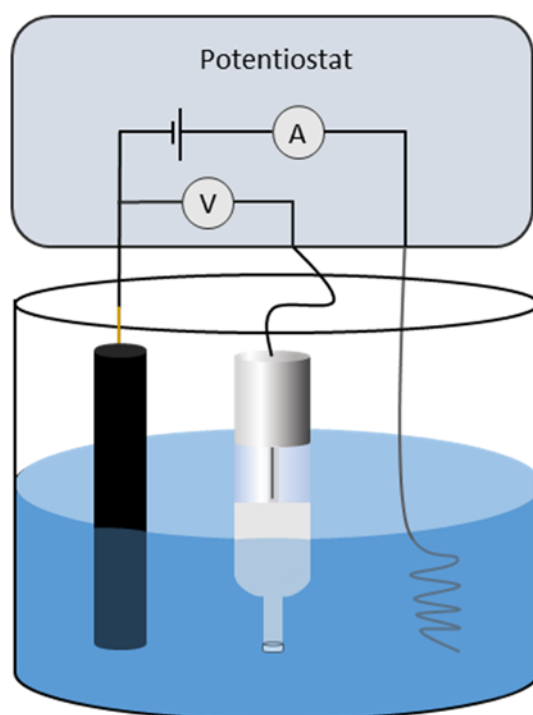
Figure 5. Three-electrode setup. The working electrode is an electrical conductor of a distinct geometry, usually an inlaid disc embedded into an insulating material. Conventional working electrode materials include: BDD, GC, Au and Pt. Two commonly used reference electrodes include silver chloride and SCE. The reference electrodes consist of an electrode immersed in a saturated electrolyte solution contained within a glass capillary. The electrode and analyte solution are in contact with the analyte solution *via* a frit. This study used an SCE (half equation Cl$^-$ (Sat)|Hg$_2$Cl$_2$(s)|Hg(l)|Pt).

1.5.3 Cyclic Voltammetry

CV is a widely used technique for studying electrochemical reactions. Firstly, a potential is applied where no electrode reaction occurs; this is the initial potential value (E_i). A triangular potential waveform is subsequently applied (Fig. 6a). Initially, the applied potential is changed linearly with time (constant scan rate) allowing the reduction or oxidation (depending on the direction of the scan) of an electroactive species once an overpotential has been reached. Once the potential region where the electrochemical reaction takes place has been transversed, the scan direction is reversed. A second peak corresponding to the oxidation or reduction of the intermediates formed in the forward scan is visible (if the redox couple are reversible or quasi-reversible). One cycle consists of both a forward and reverse sweep, which is repeated for a set number of scans.

The measured current response at the working electrode is plotted against the applied potential to produce a cyclic voltammogram (Fig. 6b). Two sources of current exist; faradaic current, which is attributed to the current flow due to ET processes; and non-faradaic current, which is the capacitive current due to the double layer charging. The important parameters in a CV are the cathodic and anodic peak currents (i_p) and the half-wave potential. The peak current for a reversible redox species, such as $Ru(NH_3)_6^{3+/2+}$, is governed by the Randles Sevcik equation (eq. 1.3) allowing the concentration of an analyte to be determined.

$$i_p = 2.69 \times 10^5 n^{\frac{3}{2}} A D^{\frac{1}{2}} v^{\frac{1}{2}} c^* \qquad \text{at T} = 25\ ^\circ\text{C} \qquad (1.3)$$

where D = diffusion coefficient (cm^2 s^{-1}), v = scan rate (V s^{-1}), and c* = bulk concentration (molcm^{-3}).
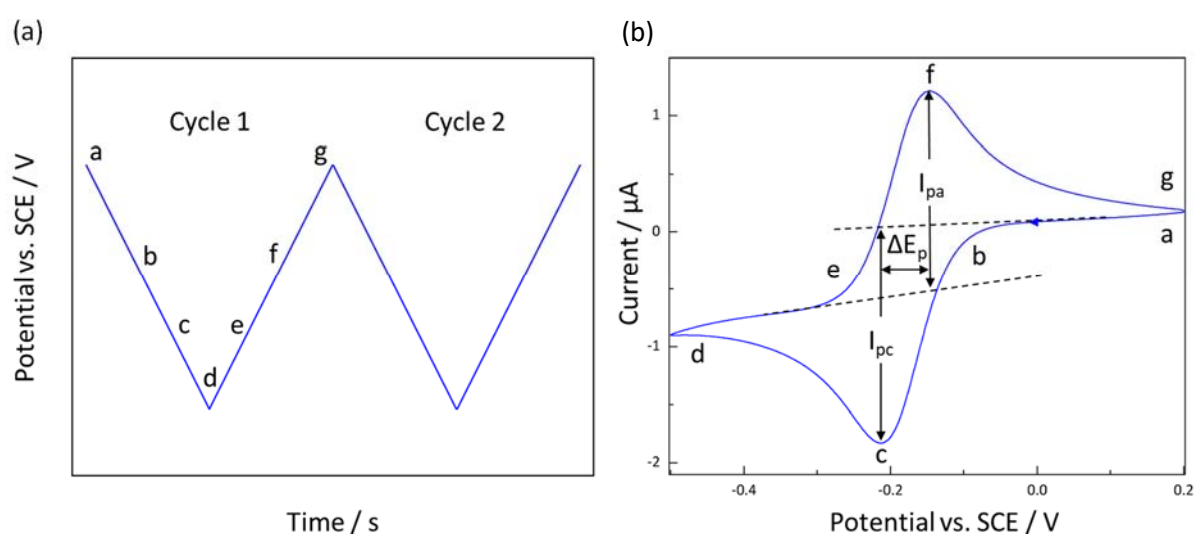
Figure 6. (a) CV triangular potential excitation waveform and (b) CV of 1 mM Ru(NH$_3$)$_6$$^{3+}$ in 0.1 M KNO$_3$ displaying characteristics of a reversible redox species. CV is defined by the scan rate, initial potential (a), switching potential (d), final potential and the total number of sweeps. The switching potential is the point where sufficient voltage has been applied to have caused either reduction (from a to d), or oxidation (from d to g).

Electrochemical reversibility can also be determined by calculating the potential peak difference ($\Delta E_P = E_{pa} - E_{Pc}$). For a reversible system, the difference is 59 mV n^{-1} at 25 °C, when this is true the rate of oxidation and reduction are equal.[103] In addition, ΔE_P should be independent of scan rate and the current passed at reduction (i_{pa}) and oxidation (i_{pc}) should increase in proportion to scan rate. The values of i_{pa} and i_{pc} should be similar in magnitude. However, if the ratio of i_{pc} and i_{pa} is greater or less than one, this indicates a semi-reversible reaction which is dependent on scan rate.

1.5.4   Differential Pulse Voltammetry

DPV is the second technique used in this study. The potential wave form is shown in Fig. 7. Small pulses of constant amplitude (usually 10 mV to 100 mV) are superimposed on a linearly increasing potential wave.   The current is measured twice; firstly, prior to the application of the pulse; and secondly, at the end of the pulse. The selection of two sampling points allows the decay of non-faradaic (charging) current.[104] The signal current obtained is the difference between these two measurements, so the differential pulse voltammogram is a plot of the differential current against the applied voltage.[105] The difference current reaches a maximum when the applied potential approaches the redox potential.

Figure 7. (a) Potential wave form for DPV and (b) differential pulse voltammogram. The peak position, peak height, and peak half-width can be changed to improve peak separation and increase sensitivity by mainly changing the amplitude and pulse width.[106] The pulse amplitude is the potential pulse height; pulse width is the duration of the potential pulse; pulse period is the time for one potential cycle; and sample period is the duration of current measurement at the end of the potential pulse.

2. Experimental Section

2.1 Materials

2.1.1 Equipment and Reagents

Milli-Q water (Millipore Corp.) with a resistivity of 18.2 MΩ cm at 25 $^{\circ}$C was used to prepare all solutions. Electrochemical measurements were conducted using solutions containing hexaamineruthenium(III) chloride $(Ru(NH_3)_6^{3+}$ (99%; Stem Chemicals, Newbury Port, MA, USA) in 0.1 M potassium nitrate (KNO_3; Fischer Scientific); caffeine (99%; Alfa Aesar, Heysham, UK), L-ascorbic acid (99.7-100.5%; Sigma-Aldrich), uric acid (≥99%; Sigma-Aldrich) and APAP (98.0-101.0%; Sigma-Aldrich) in synthetic urine (Surine^{TM}; Sigma-Aldrich); APAP in 4% BSA (≥96%; Sigma-Aldrich) and pH 7.4, 0.01 M PBS (Sigma-Aldrich); and pH 2 Carmody buffer, prepared using boric acid (99.97%; Sigma-Aldrich), citric acid (≥99.5%; Sigma-Aldrich), and tertiary sodium phosphate (≥95%; Sigma-Aldrich), following Carmody's protocol.[107] The pH meter (SevenEasy, Mettler Toledo) was calibrated using a three-point calibration using NIST standard pH solutions (pH 4 ± 0.01, pH 7 ± 0.01, and pH 10 ± 0.01; Sigma-Aldrich), following manufacturer guidelines. All electrochemical measurements were obtained using a saturated calomel reference electrode (SCE), platinum counter electrode, and a potentiostat (CHI1040a, CH Instruments, USA) as illustrated in Fig. 5. A Faraday cage was used to reduce electrical noise.

Electrodes containing varying degrees of sp^2 content were utilised throughout this study, including an all-diamond device (E6 Ltd., Ascot, UK), a GC electrode (CH Instruments Inc.,USA) and two laser ablated glass-sealed electrodes (referred to as GEN1 and GEN3, prepared in-house). All BDD electrodes possessed a 1 mm diameter, whereas the diameter of the GC electrode was 3 mm.

2.1.2 Electrode Fabrication

Laser ablated glass-sealed electrodes were fabricated using an optimised in-house method proposed by Hutton *et al.* and Ayres *et al*.[108,109] Uniform BDD discs (1 mm diameter; 470 μm thickness) were cut from a BDD wafer using a laser micromachiner (E-355H-3-ATHI-O system, Oxford Lasers). Subsequent removal of loosely contacted NDC and oxygen termination was completed *via* acid cleaning in boiling concentrated sulphuric acid (98%, Sigma-Aldrich), supersaturated with KNO_3. Reliable Ohmic connection was established by sputtering layers (Moorfields MiniLab 060 platform sputter/evaporator) of Au (400 nm) and Ti (10 nm) onto the BDD disk nucleation face and annealed in a tube furnace for 5 hours at 400 $^{\circ}$C. Following this, the BDD columns were sealed into glass capillaries

(o.d., 2 mm; i.d., 1.16 mm; Harvard Apparatus Ltd., Kent, U.K.) and polished with carbide grit paper disks and alumina paste (0.05 μm; Buehler, Düsseldorf, Germany).

NDC was subsequently introduced by laser machining a hexagonal array of 61 pits (ca. 25 μm depth, spaced 100 μm centre-to-centre, and 50 μm diameter) onto the BDD surface. The GEN1 electrode was subjected to a laser intensity of 870 J cm^{-2}, whereas an intensity of 14 J cm^{-2} was used for the GEN3 electrode. Activation of the sp^2 regions was completed by heating the electrode at ≥200 °C for 15 min in concentrated H_2SO_4 and subsequently anodically polarised under constant current conditions (+0.1 mA for 60 s) in 0.1 M room temperature H_2SO_4.

2.2 Electrode Characterisation

2.2.1 Quinone Surface Coverage

Acid cycling of all electrodes in 0.01 M H_2SO_4 was completed prior to quinone surface coverage determination to ensure comparative measurements. To guarantee this, CVs were performed from 0 V to −2 V and then 2 V, before returning to 0 V for 20 cycles to oxidise the electrode surface. Following this, CVs were carried out in pH 2 Carmody buffer, cycling from 0 to 0.7 V ($v = 0.1$ V s^{-1}). Quinone peaks were integrated to obtain the charge passed and converted to quinone surface coverage utilising equation 1.1.

2.2.2 Capacitance and Solvent Window

CVs were collected in 0.01 M PBS, 4% albumin in 0.01 M PBS (pH = 7.4) and synthetic urine (pH = 6.9) sweeping the potential between -0.1 V and 0.1 V, starting from 0 V, for 7 cycles at a scan rate of 0.1 V s^{-1}. Capacitance measurements were obtained using equation 2.1 and the second full CV.

$$C = i_{average}/vA \tag{2.1}$$

where $i_{average}$ is the current average from the forward and reverse sweep at 0 V.

The potential was subsequently swept from 0 V, down to -2 V and then to +2 V, finally returning to 0 V for 2 full cycles ($v = 0.1$ V s^{-1}). SW is defined as the potential range where the current density is no more than ±0.4 mA cm^{-2}.[110] Thus, to determine SW, the second full CV was divided by the electrode area to obtain current density. Randle Sevcik's equation (equation 1.2) was used to calculate the exact electrode area by attaining CVs of 1 mM $Ru(NH_3)_6^{3+/2+}$ in 0.1 M KNO_3 at a scan rate of 0.1 V s^{-1}. For this, the potential was swept from +0.2 V to -0.5 V for 3 full cycles.

2.3 Acetaminophen in Albumin

2.3.1 APAP Identification and Electrode Fouling

APAP was identified in the presence of PBS and 4% albumin through the analysis of solutions containing different APAP concentrations (1 mM, 0.5 mM and blank). CVs were obtained using the all-diamond device (cycling from -0.8 V to +1.2 V, starting at 0 V), GC electrode (cycling from -0.2 V to +0.7 V, starting at 0 V) and GEN3 electrode (cycling from -0.4 V to +1.2 V, starting at 0 V) at a scan rate of 0.1 V s^{-1}. Electrode fouling measurements were subsequently acquired by completing 10 full cycles and calculating the percentage drop in current between the APAP oxidation peak from the first and second scans.

2.3.2 Limit of Detection and Quantitation

CVs were obtained of APAP calibration standards, ranging from 0.5 µM to 1000 µM, prepared in 4% BSA (in 0.01 M PBS, pH 7.4). The potential was swept as described in 2.3.1 and 3 full scans were acquired. The anodic peak current of APAP was plotted against concentration to produce three calibration curves covering below therapeutic, therapeutic, and toxic APAP blood concentration levels. LOD and LOQ were calculated by multiplying the standard deviation of the regression line, by 3.3 and 10, respectively, and dividing this value by the slope of the calibration graph.[111]

2.4 Acetaminophen in Synthetic Urine

2.4.1 Distinguishing APAP from Additional Compounds

CVs of APAP (1 mM), uric acid (UA; 1 mM), caffeine (CAFF; 1 mM) and AA (1 mM) in synthetic urine were obtained using the all-diamond device. A potentiostat was used to sweep the potential from -0.4 V to +1.6 V, starting from 0 V. CVs of 0.5 mM APAP and synthetic urine were also obtained to identify APAP oxidation peaks. Electrode fouling measurements were subsequently acquired of 1 mM APAP in the presence of 1 mM caffeine by completing 10 full cycles and calculating the percentage drop in current between the paracetamol oxidation peak from the first and second scans. All electrodes were utilised for fouling measurements.

2.4.2   Limit of Detection and Quantitation

The DPV response of APAP (ranging from 0.5 µM to 1000 µM) in synthetic urine (pH = 6.9) and caffeine (1 mM) was obtained using all-diamond, GC, GEN1 and GEN3 electrodes. The parameters selected were as follows: initial potential = 0 V, final potential = 1.475 V, increment potential = 0.004 V, amplitude = 0.1 V, pulse width = 0.2 s, sample width = 0.02 s, pulse period = 0.5 s, quiet time = 2 s, and sensitivity = 1×10^{-5} A V^{-1}. The peak current was plotted against APAP concentration to produce graphs covering below therapeutic, therapeutic and toxic range of APAP content of blood. LOD and LOQ were calculated as stated in 2.3.2.

2.4.3   Optimisation

To improve the LOD and LOQ the following DPV parameters were changed: amplitude (0.05 V); pulse width (0.5 s); amplitude (0.05 V) and pulse width (0.05 s); and amplitude (0.05 V), pulse width (0.05 s), and sampling period (0.08 s). The optimised method (pulse width = 0.5 s) was selected by using the modified parameters to obtain DPVs of APAP (1 mM, 0.5 mM and blank) in synthetic urine. Following this, solutions containing 1 µM to 10 µM of APAP in synthetic urine were analysed using the optimised method and all-diamond electrode.

3.   Results and Discussion

3.1   Electrode Characterisation

3.1.1   Quinone surface coverage

Quinone surface coverage measurements were obtained by integrating the quinone oxidation peak and reported in Fig. 8. As expected, the all-diamond electrode possessed the least amount of sp^2 content and the GC electrode contained the most. All BDD material is laser micromachined to the desired geometry. This ablation process produces sp^2 carbon along the side walls which, if the solution is exposed to, results in sp^2 contamination. However, all-diamond devices were fabricated so that the BDD electrode was encased within insulating diamond, overgrown with a layer of BDD, which was polished back revealing a coplanar surface and reducing sp^2 content.[17,24]
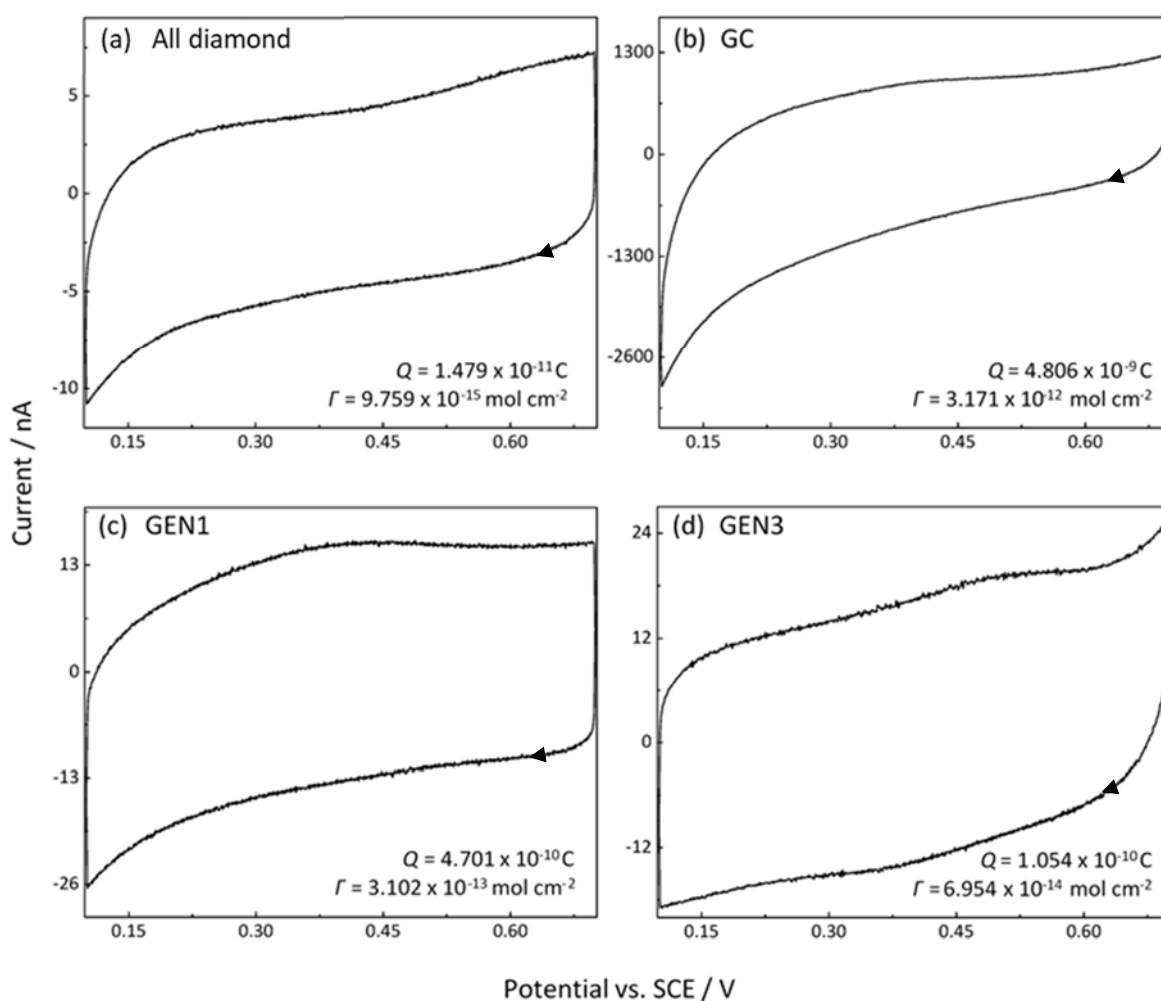

Figure 8. Quinone surface coverage measurements of (a) all-diamond, (b) GC, (c) GEN1 and (d) GEN3 electrodes. CVs were recorded of pH 2 Carmody buffer at a scan rate of 0.1 V s^{-1}.

The laser ablated electrodes possessed intermediate-levels of sp^2 content due to the fabrication process utilised. The incident laser pulse applied to produce these electrodes results in the absorption of heat energy by the surface of the material, causing ablation, which forms a highly energetic plasma. A heat-affected zone (HAZ) is subsequently produced with sufficient energy to graphitise the surface, inducing a change in the bonding of sp^3 (oxidised to sp^2). Thus, it is unsurprising that the GEN1 electrode contained more sp^2 carbon than GEN3. The higher laser intensity used to produce the GEN1 electrode resulted in a larger heat affected zone, causing more oxidation of sp^3 carbon to sp^2.

Although the GC electrode possessed the greatest sp^2 coverage, the quinone oxidation peak is difficult to identify. The higher capacitance that is associated with the electrocatalytic nature of sp^2 carbon, which is later discussed, is most likely the cause. The four electrodes selected for this study provided sufficient coverage of NDC to investigate its effects on the analysis of biological matrices.

3.1.2 Capacitance and Solvent Window

Typical SW and capacitance measurements are made using a 0.1 M KNO₃ solution.[110] However, establishing the potential range within which the electrodes can operate before synthetic urine (an artificial biological matrix) and the 4% BSA solution is electrolysed was fundamental in understanding if APAP measurement is feasible using the electrode materials selected. As shown in Fig. 9, and documented in Table 1, the capacitive current measured increased with increasing sp^2 content. The capacitance measured for the all-diamond device was approximately 3x less than the next best electrode (GEN3), suggesting the greatest usefulness for *in vivo* applications. The lower contribution of non-faradaic processes on the overall current measured indicates the ability to measure lower concentrations. No significant change was noted between the capacitance measured in PBS and albumin, which agrees with data obtained by Fagan-Murphy, *et al*.[112]

The all-diamond device also demonstrated the largest SW, suggesting the ability to analyse multiple analytes before the solvent is electrolysed, provided they are oxidised, or reduced, at different potentials. The decrease in SW with increased sp^2 content is due to oxygen reduction reactions (ORR) and sp^2 oxidation which are not observed with catalytically inert sp^3 carbon (BDD). These electrochemical processes are emphasised in the SW of PBS. Water electrolysis and ORR are both inner sphere ET processes, requiring the presence of electrocatalytic 'binding' sites on the electrode surface to mediate ET. BDD lacks these binding sites for water and oxygen. However, GC electrodes, possessing reactive quinine-like groups, enabled efficient water-electrode and oxygen-electrode interactions. As the adult human body is approximately 50-60% water,[113] reducing water electrolysis is desirable. In addition, at positive potentials, oxidative hydroquinone/benzoquinone-like ET processes occur.

Figure 9. Capacitance and SW recorded in (a) 0.01 M PBS (pH = 7.4), (b) 4% BSA in 0.01 M PBS, and (c) synthetic urine (pH = 6.9) at 0.1 V s^{-1} using all-diamond (black line), GC (red line), GEN1 (green line) and GEN3 (blue line) electrodes. GEN1 was not used for albumin and PBS studies due to insufficient time. Current density was plotted to emphasise the difference in background current. Electrode area was calculated using Ru(NH$_3$)$_6$$^{3+}$ (CVs are in the supplementary information).
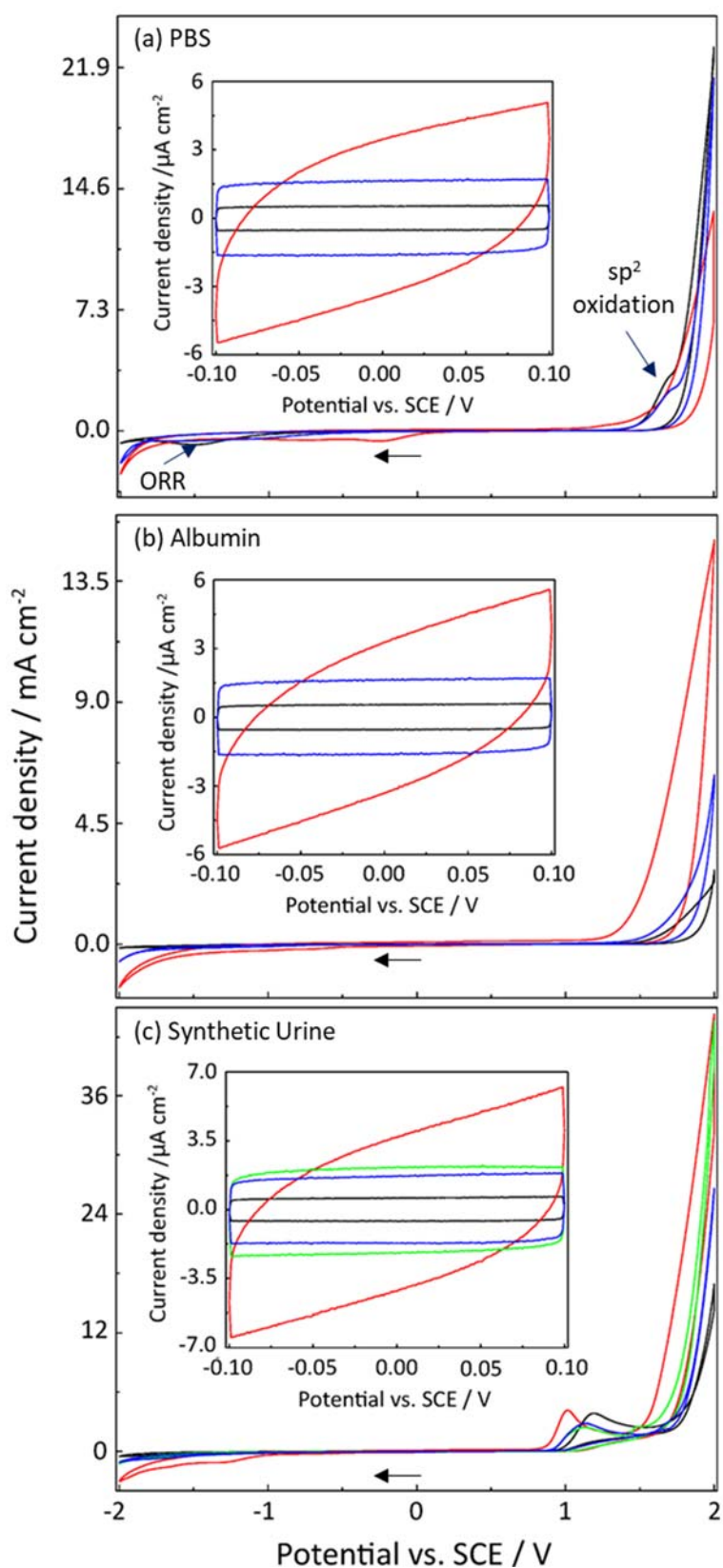
Table 1. Capacitance and SW measurements obtained using the CVs illustrated in Fig. 9 and equation 1.2. The SW of the all-diamond electrode in albumin exceeded the potential swept.

Electrode Material	Capacitance ($\mu F\ cm^{-2}$)			SW / V		
	PBS	Albumin	Synthetic urine	PBS	Albumin	Synthetic urine
All diamond	5.27	5.53	5.80	3.25	3.64+	2.94
GC	34.2	33.2	39.1	3.01	3.00	2.32
GEN1	-	-	21.9	-	-	2.70
GEN3	16.4	16.3	17.0	3.24	3.47	2.65

Despite the inert nature of BDD, a decrease in SW was noted for all electrodes in synthetic urine. This is due to the presence of an additional peak, which wasn't conclusively identified. Initially, this was thought to be urea. However, Hernández *et al.* identified that the oxidation of urea occurs at the site of oxygen evolution, involving hydroxyl radicals, in the case of BDD, and reversible adsorption onto active oxygen evolution sites in other electrodes.[114] Due to the complex nature of biological matrices, such as urine, it is difficult to ascertain the identity of this electroactive compound. One possibility is the intercalation of ions due to the high concentration of electrolytes (mainly singly-charged cations), which is known to produce additional peaks in the SW of BDD and Pt electrodes.[115] Conversely, the addition of albumin resulted in a dramatic increase in the SW, suggestive of electrode fouling. Addition of albumin resulted in the absence of ORR and sp^2 oxidation peaks in the SW of GC and GEN3 electrodes. Adsorption of the protein onto the electrode surface was the most likely cause, blocking the electrocatalytic binding sites required for the inner sphere ET processes to take place. Ferrocyanide ($Fe(CN)_6^{4-/3-}$), also an inner sphere ET, has been shown to decrease in current in the presence of BSA, supporting this postulation.[116,117]

3.2   Albumin

3.2.1   Identifying Acetaminophen using Cyclic Voltammetry

Fig. 10 illustrates the CVs obtained of APAP (1 mM and 0.5 mM) in BSA allowing the identification of the oxidation peak potential. The lack of symmetry between the oxidative and reductive segments is indicative of a quasi-reversible system. The oxidation peak of APAP is made apparent by the sharp decrease in the anodic peak current as the concentration is halved. Also, as the sp^2 content of electrodes increases, the peak potential shifts less positive, indicating that the electrocatalytic nature of sp^2 facilitates the oxidation of APAP, as less potential is required to drive the reaction. Thus, controlled addition of sp^2 content onto BDD can be tailored towards specific analytes, increasing specificity by shifting peaks until separated from interfering compounds.
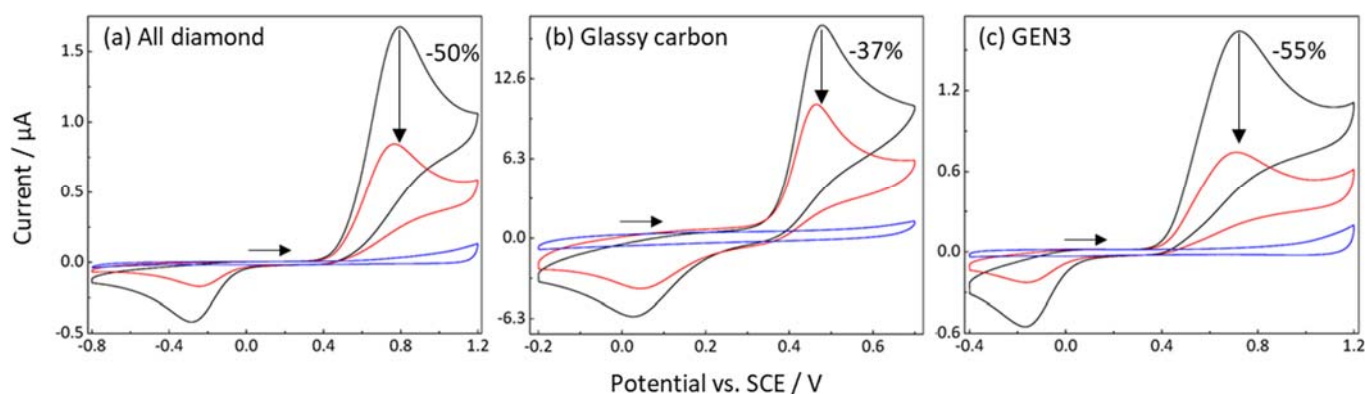
Figure 10. CVs of 1 mM (black line), 0.5 mM (red line), and blank (blue line) APAP in 4% BSA obtained with a scan rate of 0.1 V s^{-1} using (a) all-diamond, (b) glassy carbon and (c) GEN3 electrodes. There is a clear shift in the anodic peak potential when all-diamond (+0.79 V), GC (+0.48 V) and GEN3 (+0.72 V) electrodes were used.

3.2.2   Fouling

A comparison was made between the first and second oxidation segments of CVs obtained of 1 mM APAP in PBS and 4% BSA to determine the drop in current, and thus the extent of electrode fouling (Fig. 11). Although an initial large decrease in current was noted for all electrodes, the following nine full cycles exhibited a smaller drop suggesting that the electrode stabilises past the initial scan. In the presence of albumin, a greater decrease in current was observed. This is unsurprising, as albumin is a high molecular weight protein possessing both hydrophobic and hydrophilic regions, so electrode fouling was likely due to the inhibition of ET reactions on the electrode surface by the hydrophilic
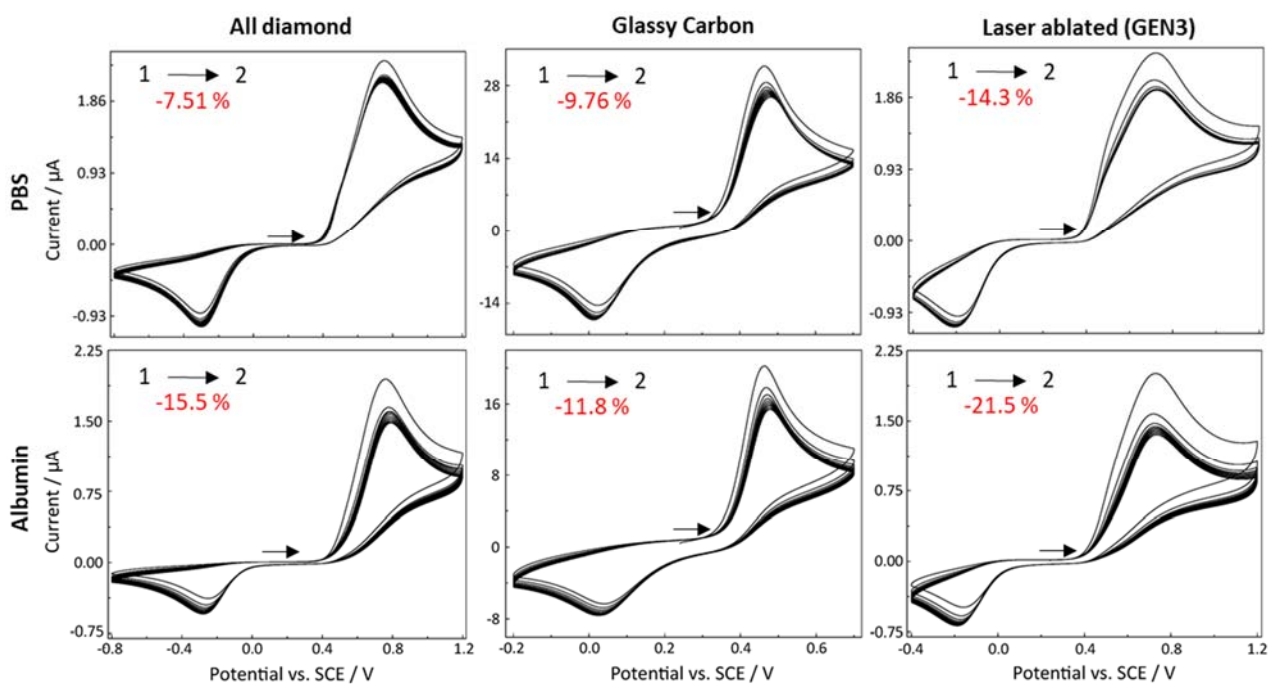
Figure 11. CVs obtained of 1mM APAP in PBS (pH = 7.4) and 4% BSA using all diamond, GC and GEN3 electrodes for investigating electrode fouling. Ten full scans were obtained at a scan rate of 0.1 V s^{-1} and electrode fouling measurements were calculated from the decrease in anodic peak current between the first and second scan.

surface-active domain. Formation of these surface protein layers is known to distort voltammetric signal and suppress electrode sensitivity.[118] Previous studies have encountered similar issues when analysing $Ru(NH_3)_6^{3+}$ in the presence of BSA, suggesting that BSA causes a drop in current for both inner $(Fe(CN)_6^{4-/3})$ and outer sphere processes.[119] The two adsorption processes suggested include simple physical adsorption and attraction and interaction of the positively charged protein and electrode interface at negative potentials.

Surprisingly, the GCE exhibited the least electrode fouling (-11.8 %), despite sp^2 content being known to increase the risk of electrode fouling. Furthermore, the GEN3 electrode demonstrated the most electrode fouling, with a 21.5% drop in current after the addition of albumin, over 7% greater than just PBS. Attenuation of the anodic peak current was likely due to the blocking of the pits introduced during electrode fabrication, resulting in less surface area for ET processes to occur. As seen with the GC electrode, sp^2 content increases the current measured, so adsorption of BSA onto the GEN3 electrode pits is expected to cause significant fouling. Hence, not only does sp^2 content have to be considered for the analysis of biological matrices, but also the method of electrode fabrication. A better understanding is required of how long-term BSA exposure will affect electrode fouling, as this could determine if unmodified electrodes are suitable for the continuous monitoring of APAP in blood.

3.2.3 Limit of Detection

CVs used to produce calibration plots of concentration versus anodic peak current are present in the supplementary information (Fig. S2), as well as the calibration plots, for the analysis of APAP (ranging from 0.5 µM to 1000 µM) in PBS (Fig. S3) and 4% BSA (Fig. S4). Three calibration graphs were produced, covering below therapeutic (0.5 µM to 25 µM), therapeutic (10 µM to 100 µM) and toxic (100 µM to 1000 µM) blood concentration ranges of APAP, which have been previously stated. Table 2 summarises the data provided by the calibration plots. LOD and LOQ values were calculated using the standard deviation and gradient of the slope from the below therapeutic (or therapeutic in the case of GC) calibration graphs. Visually, the GC electrode lacked the sensitivity to reach below therapeutic detection limits as no oxidation peaks were observed.

Table 2. Summary of data provided by the calibration graphs of APAP in PBS and BSA (Fig. S3 and S4). LOD and LOQ were calculated by multiplying the standard deviation of the slope by 3.3 and 10, respectively, and dividing it by the gradient. Values quoted in green, yellow, and red correspond with the calibration graphs produced for below therapeutic, therapeutic, and toxic APAP blood concentration levels, respectively.

Electrode	PBS			BSA		
	LOD / µM	LOQ / µM	R^2	LOD / µM	LOQ / µM	R^2
All-diamond	0.0548	0.166	0.9992	0.428	1.30	0.9520
			0.9878			0.9878
			0.9891			0.9891
GC	0.201	0.608	0.9890	0.501	1.52	0.9353
			0.9845			0.9959
GEN3	0.885	2.68	0.8740	0.652	1.97	0.9625
			0.8263			0.9762
			0.9851			0.9939

Along with achieving the most reproducible results and best correlation between concentration and peak anodic current (based on R^2 values) over a large concentration range, the all-diamond device demonstrated the lowest LOD and LOQ. This is most likely attributed to the intrinsically low background current of sp^3 carbon. However, it was the GEN3 electrode which demonstrated the worst calculated LOD and LOQ, despite the GCE possessing higher sp^2 content and capacitance. Nevertheless, no oxidation peak was observed below 5 µM APAP in PBS (and 10 µM APAP in BSA) when using a GCE, suggesting that the calculated LOD is an overestimation, whereas visually the LOD of GEN3 was 1 µM (and 5 µM in BSA). Contrary to all other LOD calculations, the therapeutic calibration graph was used to calculate the LOD of APAP using the GCE. Thus, the overestimated LOD is likely due to a reduced standard deviation of the gradient as the concentrations measured are farther from the LOQ. Future use of S/N ratio of LOD calculation could prevent overestimations.[111] The abnormally high detection limits of the GEN3 electrode could also be due to the pits introduced during the fabrication process. This speculation is reasonable as the LOD, LOQ and R^2 value all improved upon addition of BSA. Adsorption of BSA onto the electrode surface is thought to have prevented the efficient ET between APAP and sp^2 content present in the pits. Despite these improvements, the LOD and LOQ were still worse than all other electrodes.

Upon addition of BSA, the performance of all electrodes, excluding GEN3, decreased. The LOD and LOQ increased by roughly one-order of magnitude and linearity decreased. Although the R^2 value of the GEN3 electrode appears to be the best at below therapeutic concentrations, this is deceiving as no peak was observed below 5 µM, so the calibration plot was made with only 3 data points (one of which possessed a large standard deviation). Inevitably, the correlation between concentration and peak current worsened (reduced R^2 value) with decreasing concentration, as the LOQ was approached. Despite this, all electrodes demonstrated sufficient LOD, LOQ and linear dynamic range for the quantitative analysis of APAP in the presence of albumin in both the therapeutic and toxic APAP blood concentration.

The all-diamond electrode is expected to be most suited for the analysis of blood, with LOD and LOQ within the therapeutic blood concentration range of APAP and exhibiting less fouling than the GEN3 electrode. These results suggest that lower sp^2 content is desirable to minimise background current and thus maximise sensitivity, and that the fabrication of laser ablated electrodes pose issues. Table 3 illustrates that the LOD and linear range achieved using the all-diamond electrode in this study are comparable with those in literature but does not surpass modified electrodes. However, it should be noted that the studies referenced employed the use of additional techniques (e.g. square-wave voltammetry) and did not analyse solutions containing albumin; however, some analysed synthetic urine samples. Nevertheless, unmodified BDD has demonstrated the performance capabilities required

to measure APAP concentrations in blood, using albumin as proof-of-concept, without the need for costly and complicated modification procedures.

Table 3. Comparison of various electroanalytical methods for the determination of APAP.

Electrode	Linear range / µM	Detection limits / µM	Reference
BDD	0.5 - 1000	0.389	This study
BDD	0.01 - 0.1	0.81	83
BDD modified with Nafion and lead films	0.5 - 200	0.17	84
BDD	0.1 - 0.8	10	120
BDD	0.2 - 60	0.11	88
MWCNTs/GCE	0.5 – 1000	0.05	46
SWCNT/CCE	0.2 – 150	0.12	69
Modified graphene oxide electrode	0.10-2.9	0.0067	81

3.3   Synthetic Urine

3.3.1   *Distinguishing Pharmaceutically Active Compounds*

CVs of APAP in synthetic urine and in the presence of caffeine (CAFF), uric acid (UA) and AA were obtained (Fig. 12). A comparison between CVs obtained from 1 mM and 0.5 mM APAP and a synthetic urine blank revealed the presence of two characteristic oxidation peaks with the sole addition of APAP. A drop in current at +0.35 V and +0.85 V was visible with decreasing APAP concentration. Initially, one of the peaks was thought to be UA. However, oxidation of UA was found to occur at +0.57 V, directly in-between the two peaks associated with APAP. Caffeine was easily distinguished from APAP and the contents of synthetic urine, with an oxidation peak at +1.46 V, demonstrating the exceptional specificity of the electrochemical methods of analysis used in this study. Conversely, the addition of 1 mM AA to APAP and caffeine enhanced the anodic peak current of the first peak (+0.46 V) of APAP. Previous studies have suggested that at pH values above 7 the oxidation peaks for AA and APAP are indistinguishable indicating that the enhanced peak is likely APAP.[67] Thus, the peak at +0.46 V was used for all subsequent measurements. The second peak is thought to be the oxidation of
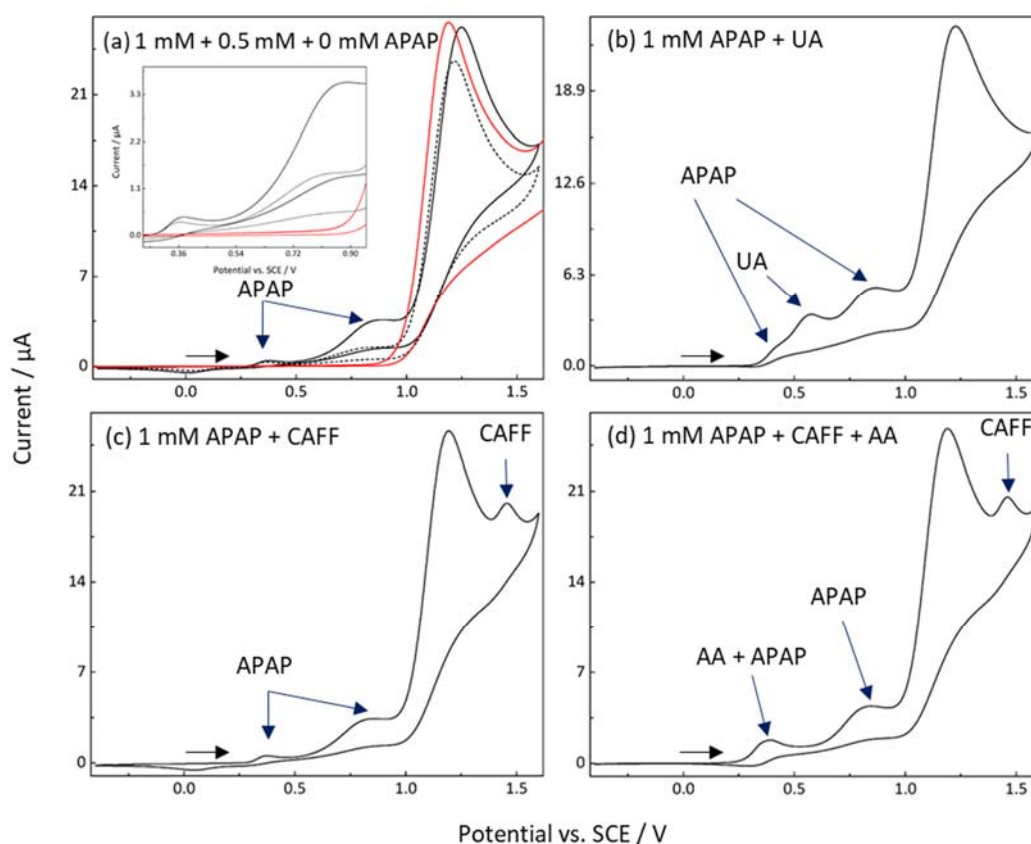

Figure 12. Comparison of CVs obtained with added biochemical and pharmaceutically active compounds to synthetic urine (pH = 6.9). All CVs were obtained at a scan rate of 0.1 V s^{-1}. (a) Identification of APAP was completed by obtaining CVs of 1 mM (black solid line), 0.5 mM (black dashed line) and blank (red) APAP.

a product formed from the reaction between APAP and the contents of synthetic urine. However, due to the complex nature of biological matrices, it is difficult to determine the exact cause. The presence of two characteristic oxidation peaks is very advantageous and, if also present in real urine samples, would allow APAP to be identified with greater certainty.

3.3.2   Electrode Fouling

As completed previously, CVs (10 full cycles at a scan rate of 0.1 V s^{-1}) were obtained to determine the extent of electrode fouling caused by synthetic urine (Fig. 13) by determining the percentage drop in current between the first and second oxidation peak of APAP. The GEN1 electrode, possessing the second most sp^2 content, exhibited the lowest drop in current (-13.5 %). In addition, contrary to all other electrodes, the current remained stable after the first scan. This unusual behaviour is likely caused by incompletion of acid cycling following the fabrication of the electrode resulting in the incomplete removal of any loosely bound sp^2 groups and other material deposited from the fabrication process, reducing the surface area for ET processes to occur. This assumption is also supported by the low currents measured (lowest of all electrode), despite the increased incorporation of sp^2 groups.
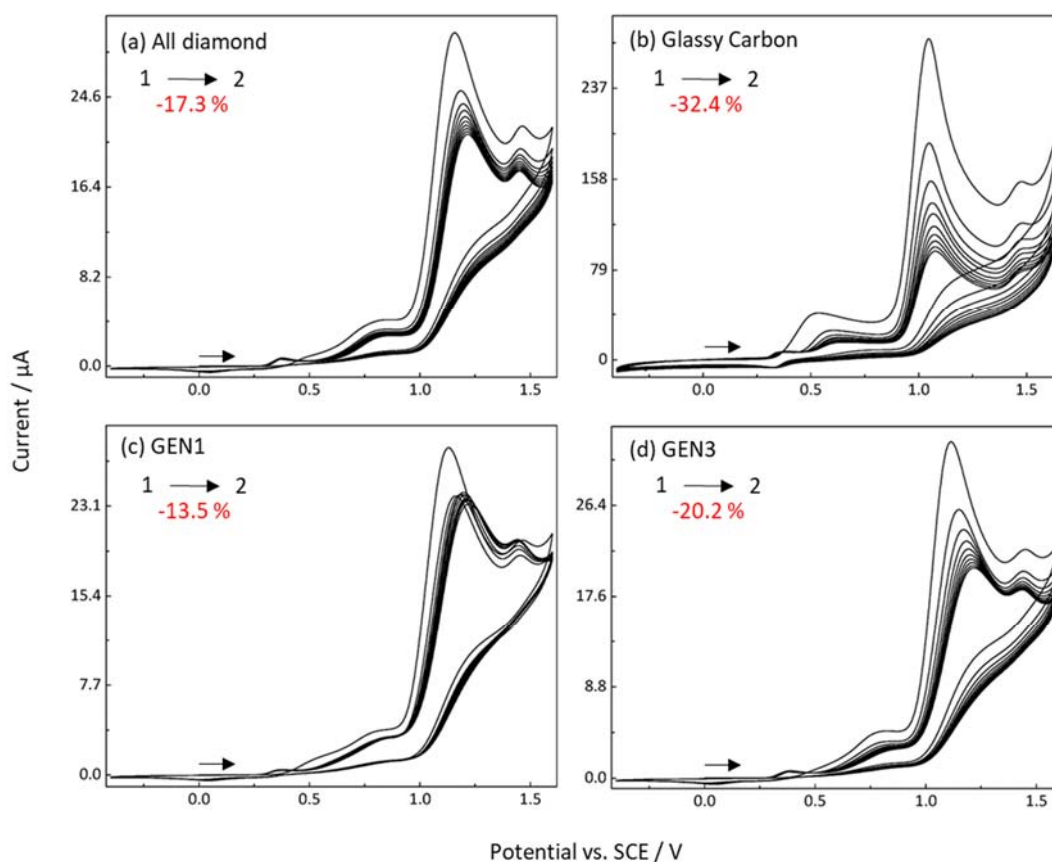

Figure 13. CVs obtained of synthetic urine containing 1 mM APAP and 1mM caffeine using (a) all-diamond, (b) GC, (c) GEN1 and (d) GEN3 electrodes for investigating electrode fouling. Ten full scans were obtained at a scan rate of 0.1 V s^{-1} and electrode fouling measurements were calculated from the decrease in current between the first and second oxidation segments.

Excluding the results obtained for the GEN1 electrode, an increase in sp^2 content led to an increased amount of fouling, which continued to increase after each cycle. Although the all-diamond electrode possessed the next lowest amount of fouling, a 17.3% drop in current was still noted, with the continuous decrease in current after each cycle. Transportation of waste material is one of the important biological functions of blood. Thus, extensive fouling of the same components found in urine could inhibit the continuous monitoring of APAP in blood. For example, the most abundant compound in urine, urea, is known to adsorb onto the electrode surface.[114] One possible solution is to simply conduct all calculations using the second full scan as the drop in current is reduced between all subsequent cycles.

3.3.3   Limit of Detection

DPVs used to produce calibration plots of concentration versus anodic peak current are present in the supplementary information (Fig. S5), as well as the calibration plots (Fig. S6), for the analysis of APAP (0.5 µM to 1000 µM) in synthetic urine. DPV was used instead of CV as lower LOD are attainable. To produce results comparable to those of APAP in BSA, the same concentration ranges were selected (below therapeutic, therapeutic, and toxic APAP blood concentration levels). This was used to assess if quantification of APAP was still possible in blood, at the therapeutic and toxic level, even in the presence of potentially interfering compounds found in urine. The calibration graph below therapeutic levels encompass the assumed APAP concentrations present in urine after the consumption of therapeutic and exceeded doses, thus indicating if suitable for APAP measurements in urine. Therapeutic concentrations of APAP in urine range between 0.3 µM and 6.5 µM (1-5% of blood concentration).[121]

In comparison with the calibration graphs produced during the analysis of APAP in BSA, a significant improvement was found in the overall reproducibility of results obtained using the GEN3 electrodes. Both GEN1 and GEN3 demonstrated the greatest reproducibility, especially at lower concentrations. Table 2 contains a summary of the data provided by the calibration graphs, which was compared to the data obtained during the analysis of APAP in 4% BSA. The LOD and LOQ of GEN3 improved from 0.652 µM and 1.97 µM to 0.286 µM and 0.867 µM, respectively. The LOD and LOQ of the GCE and all-diamond electrodes also improved by roughly 2-fold and 10-fold, respectively, and linearity was improved (except at higher concentrations for the all-diamond device). The significant improvement in the performance of the GEN3 and GC electrodes was thought to be caused by the lack of large molecular weight proteins present in urine, which was shown to cause extensive fouling in electrodes with high sp^2 content, as proteins do not pass the glomerular capillary wall (glomerular filtration barrier).[122] Furthermore, DPV also enhances sensitivity by allowing the decay of non-faradaic (charging) current. The all-diamond device may be more beneficial for the analysis of APAP in urine

of patients containing defective GFB and kidney disease where abnormal protein concentrations are found in urine.[122]

Table 4. Summary of data provided by the calibration graphs of APAP in synthetic urine (Fig. S6). LOD and LOQ were calculated by multiplying the standard deviation of the slope by 3.3 and 10, respectively, and dividing it by the gradient. Values quoted in green, yellow and red correspond with below therapeutic, therapeutic and toxic APAP blood concentration levels, respectively.

Electrode	LOD / μM	LOQ / μM	R^2		
All diamond	0.0487	0.148	0.9996	0.9830	0.8926
GC	0.266	0.806	-	0.9809	0.9992
GEN1	0.0276	0.0837	0.9999	0.9994	0.9934
GEN3	0.286	0.867	0.9852	0.9980	0.9651

The GEN1 electrode also obtained LOD and LOQ values unsurpassed by any other electrode despite containing the second most sp^2 content and second highest capacitance. This indicates that the importance of sp^2 content for the analysis of APAP in biological matrices cannot simply be answered with these electrodes. The manner of electrode fabrication has also been witnessed as a contributing factor. Moreover, depending on how the BDD has been grown and subsequently treated, the resulting material properties could also vary.[24] The fabrication of all-diamond devices results in a surface that is very different from the other electrodes used, which is also likely contributing to the results obtained. Even so, the LOD, LOQ and linearity achieved at lower concentrations using the all-diamond electrode were exceptional. Furthermore, no significant interference in the anodic peak current was found despite the complex nature of urine, suggesting that these materials possess the specificity, sensitivity and linear dynamic range suitable for *in vitro* monitoring of APAP in human urine samples.

All electrodes demonstrated the necessary performance criteria to continuously monitor APAP in blood, even in the presence of compounds that are present in synthetic urine, caffeine and albumin. However, only the all-diamond and GEN1 electrodes possessed the performance characteristics required for measuring APAP concentration levels in urine following consumption of therapeutic doses. Detection limits of the GC and GEN3 electrodes were hindered due to the presence of a larger peak adjacent to the APAP oxidation peak (+0.40V), which was thought to be due to the intercalation of ions.

Thus, peak deconvolution may help to improve the LOQ and LOD. The position of this second peak was shifted to less positive potentials with increasing sp^2 content, most likely from the enhanced electrocatalytic activity. This demonstrates again that specificity can be enhanced by changing sp^2 content. The DPV of the GC electrode (Fig. S5b) only possessed a single peak suggesting the inability to separate the two peaks. However, this did not seem to affect the electrodes performance.

3.3.4 Optimisation

Optimisation of the previous method was attempted by adjusting the DPV parameters, as shown in Fig. S7 in the supplementary information. The parameters of most usefulness were amplitude and pulse width. Increasing the amplitude had the effect of increasing anodic peak current, thus providing enhanced sensitivity, however, poor separation was observed with the adjacent peak. Therefore, a compromise between sensitivity and selectivity is required. The optimised method differed by only an increase in pulse width which enhanced peak current and improved peak separation.

Better separation is visible between the oxidation peak of APAP (shifted to +0.42 V) and the adjacent peak (Fig. 14). The asymmetry of the peak in the optimised DPV of the GCE suggests overlapping of the two peaks. This inability to resolve two peaks indicates that GC may not be suitable for *in vivo* analysis due to a lack of selectivity. The optimised method also reduced the analysis time from 3 min to 1 min by reducing the potential window scanned. Although this is faster than the conventional methods used,[123–125] this could be further improved with the use of square-waved voltammetry.[87] DPV has demonstrated here how a few parameters can be altered with ease to enhance sensitivity and selectivity, which could quickly and easily be changed to analyse additional compounds. Such a powerful tool could lead to the development of future multi-purpose sensors allowing the detection of APAP, whilst simultaneously monitoring biological responses through the detection of further biochemicals.
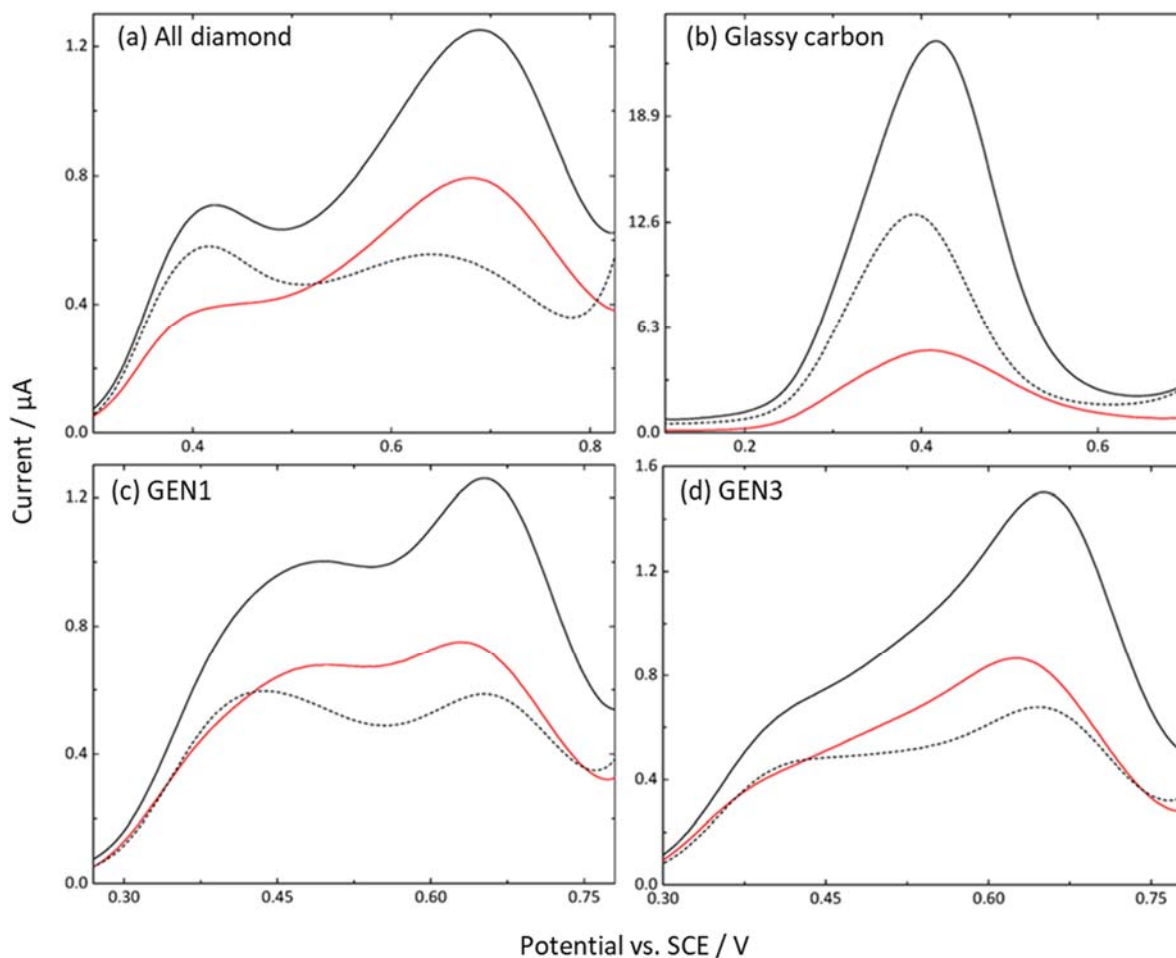
Figure 14. DPV response of 1 mM APAP before (red line), and after optimisation (solid black line). The concentration was halved (black dashed line), to determine if separation was still sufficient. Initial operating parameters were initial potential = 0 V, final potential = 1.475 V, increment potential = 0.004 V, amplitude = 0.1 V, pulse width = 0.2 s, sample width = 0.02 s, pulse period = 0.5 s, quiet time = 2 s, and sensitivity = 1×10^{-5} A/ V. However, the optimised method possessed a pulse width of 0.5 s.

Due to time constraints, this optimised method was solely used on the all-diamond electrode to plot a calibration graphs covering the therapeutic and toxic range of APAP in urine (Fig. 15). Good correlation between concentration and peak anodic current was noted (R^2 = 0.9931). However, the reproducibility was untested due to insufficient time. The LOD and LOQ values obtained, 0.137 μM and 0.417 μM, respectively, are worse than previously calculated. Two possible reasons for this include: (1) the absence of triplicate measurements, and (2) the previous calibration graphs may have been statistically skewed by the measurements of APAP concentrations that are too high. Nevertheless, the LOD and LOQ values are sufficient for the detection and quantification of APAP in urine, suggesting that all-diamond electrodes can be used for the quantification of APAP in biological matrices using DPV.
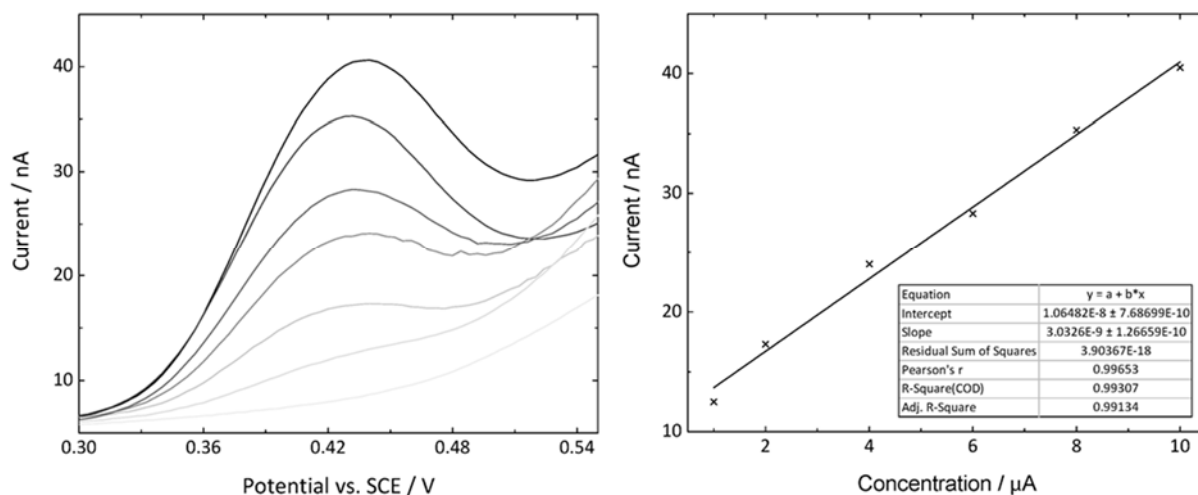
Figure 15. Use of optimised DPV method for the analysis of APAP in synthetic urine with concentrations ranging from 1 µM to 10 µM, covering most of the therapeutic concentration range in urine (1-5% of blood therapeutic concentration). Insufficient time was provided to repeat these measurements. Decreasing concentration is represented by decreasing grayscale.

4.   Conclusion

This proof-of-concept study has successfully exploited the use of electroanalytical methods for *in vitro* measurements of APAP in synthetic urine and albumin solutions, providing the necessary basis for future *in vivo* work. BDD and GC electrodes containing varying sp^2 content revealed the ability to shift the oxidation potential of APAP and adjacent peaks demonstrating excellent specificity. Furthermore, DPV studies possessed the ability to enhance sensitivity and selectivity of peaks simply by changing two parameters, amplitude and pulse width, without the need for costly and complicated electrode functionalisation processes. Such capabilities could lead to the development of multipurpose BDD *in vivo* sensors, allowing the detection of APAP, whilst simultaneously monitoring biological responses through the detection of further biochemicals. Initial studies have already begun to prove this through the simultaneous detection of caffeine, uric acid and APAP using CV.

Electrode fabrication, treatment and sp^2 surface coverage were also found to significantly influence performance including LOD, LOQ, reproducibility and fouling during quantitative analysis of APAP, mainly in albumin. Thus, electrode fabrication should be tailored towards the biological matrices analysed. For example, albumin surface adsorption onto electrocatalytically active sp^2 groups and pits introduced through laser ablation methods is likely to prevent the use of laser ablated BDD electrodes for *in vivo* measurements in blood. However, laser ablated electrodes demonstrated exceptional LOD, LOQ, reproducibility and linearity in synthetic urine due to the low concentration of proteins present.

Unmodified BDD has been revealed as a prospective material for *in vivo* measurements of APAP in blood, obtaining the necessary detection and quantification limits, in albumin, required for monitoring of therapeutic concentrations in blood. Moreover, the rapid detection of minute concentration of APAP in synthetic urine, obtaining two identifiable oxidation peaks, indicate potential use for *in vitro* measurements of urine samples within shorter analysis times compared to conventional methods.

Although this *in vitro* work has provided significant insight into the possible applications of BDD as a biological sensor, *in vivo* studies are still required to continuously and realistically monitor biological events *in situ* and capture the entire complexity of intact organ systems. However, this work has paved the way for future *in vivo* research using BDD which, if successful, could revolutionise personalised medicine by ensuring that the correct drug is provided at the right time and dose.

5. Future Work

Future studies should be directed on utilising all-diamond devices on synthetic, or human blood to investigate the full complexity of biological matrices and their effects on electrode performance. This study illustrated the significant effects that a single protein can have on an electrode's performance. Coagulation factors, such as fibrinogen, are also present in blood, so should be investigated. Although no studies were found on the influence of fibrinogen on electrode performance, adsorption of fibrinogen onto polycrystalline diamond is known.[126]

Future measurements of APAP metabolites in synthetic urine, or human urine, should be undertaken to determine potential interferences. Although previous studies suggest that the major conjugated sulphates and glucuronide metabolites appear at less positive potentials,[67] this could be dependent on diamond electrode surfaces and sp^2 content.

Additional pharmaceutical compounds will be investigated, such as aspirin and ibuprofen, to investigate if BDD can be used for the simultaneous detection of multiple components. Furthermore, both detection and quantification of these analytes should be completed to determine if a single electrode can be used to quantify multiple drugs. This would exceed the limitations of multiple current sensors. Furthermore, spike recovery tests will be completed to test the accuracy of this method and square-wave voltammetry will be attempted to reduce analysis time.

Finally, miniaturisation of BDD electrodes is vital for use as an *in vivo* sensor. Future studies should focus on how miniaturisation of electrodes affects performance. The decreased surface area could reduce currents measured hindering the LOD and LOQ. However, this may not be the case as a change in diffusion profile will occur from planar to hemispherical/ spherical, which will also influence the results. Once sufficient progress is made *in vivo* sensing can be considered.

6.   References

1   C. Brett and A. Brett, in *Electroanalysis*, eds. R. Compton, S. Davies, J. Evans and L. Gladden, Oxford University Press, Oxford, 1st edn., 2005, pp. 1–7.

2   D. Krause, in *Electrochemistry of Glasses and Glass Melts, including Glass Electrodes*, eds. H. Bach and F. Baucke, Springer, Berlin Heidelberg, 1st edn., 2001, pp. 1–3.

3   A. Bard and L. Faulkner, *Int. J. Hydrog. Energy*, 1995, **20**, 835–844.

4   S. Trasatti, 1995, **20**, 835–844.

5   G. Hanrahan, D. Patil and J. Wang, *J Env. Monit.*, 2004, **6**, 657–664.

6   A. Hagfeldt, G. Boschloo, L. Sun, L. Kloo and H. Pettersson, *Chem. Rev.*, 2010, **110**, 6595–6663.

7   J. Wang, *Biosens. Bioelectron.*, 2006, **21**, 1887–1892.

8   J. Frew and H. Hill, *Anal. Chem.*, 1987, **59**, 933A–944A.

9   S. Vashist, A. Venkatesh, K. Mitsakakis, G. Czilwik, G. Roth, F. Stetten and R. Zengerle, *Bionanoscience*, 2012, **2**, 115–126.

10   C. Ogawa, A. Oki, M. Takai, M. Nagai, H. Hisamoto and Y. Horiike, *Jpn. J. Appl. Phys.*, 2006, **45**, 4241–4247.

11   C. Torres, *Curr. Opin. Biotechnol.*, 2014, **27**, 107–114.

12   J. Pickup, *Trends Biotechnol*, 1993, **11**, 285–291.

13   S. Griveau, C. Dumezy, J. Seguin, G. Chabot, D. Scherman and F. Bedioui, *Anal. Chem.*, 2007, **79**, 1030–1033.

14   K. Wassum, V. Tolosa, J. Wang, E. Walker, H. Monbouquette and N. Maidment, *Sensors (Basel)*, 2008, **8**, 5023–5036.

15   M. Eckert, P. Vu, K. Zhang, D. Kang, M. Ali, C. Xu and W. Zhao, *Theranostics*, 2013, **3**, 583–594.

16   M. Hamburg and F. Collins, *N. Engl. J. Med.*, 2010, **363**, 301–304.

17   F. Patolsky, G. Zheng and C. Lieber, *Nat. Protoc.*, 2006, **1**, 1711–1724.

18   D. Rissin, C. Kan, T. Campbell, S. Howes, D. Fournier, L. Song, T. Piech, P. Patel, L. Chang, A. Rivnak, E. Ferrell, J. Randall, G. Provuncher, D. Walt and D. Duffy, *Nat. Biotechnol.*, 2010, **28**, 595–599.

19   N. Oliver, C. Toumazou, A. Cass and D. Johnston, *Diabet. Med.*, 2009, **26**, 197–210.

20   G. Wilson and R. Gifford, *Biosens. Bioelectron.*, 2005, **20**, 2388–2403.

21   D. Thévenot, K. Toth, R. Durst and G. Wilson, *Biosens. Bioelectron.*, 2001, **16**, 121–131.

22   M. Eckert and W. Zhao, *Interface Focus*, 2013, **3**, 20130014.

23   B. Ferguson, D. Hoggarth, D. Maliniak, K. Ploense, R. White, N. Woodward, K. Hsieh, A. Bonham, M. Eisenstein, T. Kippin, K. Plaxco and H. Soh, *Sci. Transl. Med.*, 2013, **5**,

213ra165.

24   J. Macpherson, *Phys. Chem. Chem. Phys.*, 2015, **17**, 2935–2949.

25   Z. Ayres, A. Borrill, J. Newland, M. Newton and J. Macpherson, *Anal. Chem.*, 2016, **88**, 974–980.

26   O. Williams, M. Nesladek, M. Daenen, S. Michaelson, A. Hoffman, E. Osawa, K. Haenen and R. Jackman, *Diam. Relat. Mater.*, 2008, **17**, 1080–1088.

27   T. Watanabe, Y. Honda, K. Kanda and Y. Einaga, *Phys. status solidi*, 2014, **211**, 2709–2717.

28   Z. Ayres, S. Cobb, M. Newton and J. Macpherson, *Electrochem. commun.*, 2016, **72**, 59–63.

29   H. Patten, L. Hutton, J. Webb, M. Newton, P. Unwin and J. Macpherson, *Chem. Commun.*, 2015, **51**, 164–167.

30   N. Ferreira, E. Abramof, E. Corat and V. Trava-Airoldi, *Carbon N. Y.*, 2003, **41**, 1301–1308.

31   J. Park, J. Galligan, G. Fink and G. Swain, *Anal. Chem.*, 2006, **78**, 6756–6764.

32   J. Brock and J. Tan, *Br. J. Pharmacol.*, 2004, **142**, 267–274.

33   G. Swain and R. Ramesham, *Anal. Chem.*, 1993, **65**, 345–351.

34   B. Patel, X. Bian, V. Quaiserová-Mocko, J. Galliganb and G. Swain, *Analyst*, 2007, **132**, 41–47.

35   B. Patel, *Analyst*, 2008, **133**, 516–524.

36   X. Bian, B. Patel, X. Dai, J. Galligan and G. Swain, *Gastroenterology*, 2008, **133**, 516–524.

37   H. Zhao, X. Bian, J. Galligan and G. Swain, *Diam. Relat. Mater.*, 2010, **19**, 182–185.

38   Y. Singh, L. Sawarynski, H. Michael, R. Ferrell, M. Murphey-Corb, G. Swain, B. Patel and A. Andrews, *ACS Chem Neurosci*, 2010, **1**, 49–64.

39   J. Halpern, S. Xie, G. Sutton, B. Higashikubo, C. Chestek, H. Lu, H. Chiel and H. Martin, *Diam. Relat. Mater.*, 2006, **15**, 183–187.

40   B. Patel, J. Galligan, G. Swain and X. Bian, *Neurogastroenterol. Motil.*, 2008, **20**, 1243–1250.

41   S. Fierro, M. Yoshikawa, O. Nagano, K. Yoshimi, H. Saya and Y. Einaga, *Sci. Rep.*, 2012, **2**, 901.

42   S. Fierro, R. Seishima, O. Nagano, H. Saya and Y. Einaga, *Sci. Rep.*, 3AD, **2013**, 3257.

43   E. Bitziou, D. O'Hare and B. Patel, *Anal. Chem.*, 2008, **80**, 8733–8740.

44   H. Dong, S. Wang, J. Galligan and G. Swain, *Front. Biosci.*, 2011, **3**, 518–540.

45   P. Daneshegar, A. Moosavi-Movahedi, P. Norouzi, M. Ganjali, M. Farhadi and N. Sheibanid, *J. Braz. Chem. Soc.*, 2012, **23**, 315–321.

46   L. Chunya, Z. Guoqing, Y. Qingdan and L. Jianjie, *Bull. Korean Chem. Soc.*, 2006, **27**, 1854–1860.

47   D. Davidson and W. Eastham, *Br. Med. J.*, 1966, **2**, 497–499.

48   J. Mitchell, D. Jollow, Potter, D. Davis, J. Gillette and B. Brodie, *J. Pharmacol. Exp. Ther.*, 1973, **187**, 185–194.

49   J. Herrero, I. Castellano, J. Gómez-Martino, R. Novillo and A. Covarsí, *Nefrologia*, 2001, **21**,

592–595.

50   C. Sy-Jou, L. Chin-Sheng, H. Chin-Wang, L. Cheng-Li and K. Chia-Hung, *Med.*, 2015, **94**, e1195.

51   D. Gunnell, V. Murray and K. Hawton, *Suicide Life-Threatening Behav.*, 2000, **30**, 313–326.

52   M. Schulz and A. Schmoldt, *Pharmazie*, 2003, **58**, 447–474.

53   L. Prescott, *Br. J. Clin. Pharmacol.*, 1980, **10**, 291S–298S.

54   D. Jones, G. Sundby, K. Ormstad and S. Orrenius, *Biochem. Pharmacol.*, 1979, **28**, 929–935.

55   P. Nagaraja, K. Murthy and K. Rangappa, *J. Pharm. Biomed. Anal.*, 1998, **17**, 501–506.

56   J. Staden and M. Tsanwani, *Talanta*, 2002, **58**, 1095–1101.

57   J. Vilchez, R. Blanc, R. Avidad and A. Navalón, *J Pharm Biomed Anal*, 1995, **13**, 1119–1125.

58   A. Moreira, H. Oliveira, T. Atvars, I. Dias, G. Neto, E. Zagatto and L. Kubota, *Anal. Chim. Acta*, 2005, **539**, 257–261.

59   D. Easwaramoorthy, Y. Yu and H. Huang, *Anal. Chim. Acta*, 2001, **439**, 95–100.

60   T. King, C. Mann and T. Vickers, *J. Pharm. Sci.*, 1985, **74**, 443–447.

61   M. Ramos, J. Tyson and D. Curran, *Anal. Chim. Acta*, 1998, **364**, 107–116.

62   G. Lau and J. Critchley, *J Pharm Biomed Anal*, 1994, **12**, 1563–1572.

63   W. Peng, T. Li, H. Li and E. Wang, *Anal. Chim. Acta*, 1994, **298**, 415–421.

64   G. Burgot, F. Auffret. and J. Burgot, *Anal. Chim. Acta*, 1997, **343**, 125–128.

65   M. Srivastava, S. Ahmad, D. Singh and I. Shukla, *Analyst1*, 1985, **110**, 735–737.

66   T. Perez-Ruiz, M.-L. Carmen, V. Tomas and R. Galera, *J. Pharm. Biomed. Anal.*, 2005, **38**, 87–93.

67   I. Navarro, D. Gonzalez-Arjona, R. E and M. Ruesda, *J. Pharm. Biomed. Anal.*, 1988, **6**, 969–976.

68   O. Lau, S. Luk and Y. Cheung, *Analyst*, 1989, **114**, 1047–1051.

69   B. Habibi, M. Jahanbakhshi and M. Pournaghi-Azar, *Anal. Biochem.*, 2011, **411**, 167–175.

70   R. Hargreaves, J. Evans, D. Pelling and K. Butterworth, *Toxicol. Appl. Pharmacol.*, 1982, **64**, 380–392.

71   V. Das Gupta, *J. Pharm. Sci.*, 1980, **69**, 110–113.

72   S. Mayanna and B. Jayaram, *Analyst*, 1981, **106**, 729–732.

73   R. Williams, D. Baker and J. Schmit, *J. Chromatogr. Sci.*, 1973, **11**, 618–624.

74   B.-S. He and J.-X. Zhang, *Sensors*, 2017, **17**, E1549–E1563.

75   B. Hansen and G. Dryhurst, *J. Electroanal. Chem. Interfacial Electrochem.*, 1971, **30**, 417–426.

76   R. Nunes and É. Cavalheiro, *J. Braz. Chem. Soc*, 2012, **23**, 670–677.

77   N. Spãtaru, B. Sarada, D. Tryk and A. Fujishima, *Electroanalysis*, 2002, **14**, 721–728.

78   J. Benschoten, J. Lewis, W. Heineman, D. Roston and P. Kissinger, *J. Chem. Educ.*, 1983, **60**, 772–776.

79   Y. Li and S.-M. Chen, *Int. J. Electrochem. Sci.*, 2012, **7**, 2175–2187.

80   S. Ghoreishi, M. Behpour, E. Hajisadeghian and M. Golestaneh, *J. Chil. Chem. Soc.*, 2013, **58**, 1513–1516.

81   J. Li, W. Sun, X. Wang, H. Duan, Y. Wang, Y. Sun, C. Ding and C. Luo, *Anal. Bioanal. Chem.*, 2016, **408**, 5567–5576.

82   B. Lourenc, R. Medeiros, R. Rocha-Filho, L. Mazoa and O. Fatibello-Filho, *Talanta*, 2009, **78**, 748–752.

83   C. Radovan, C. Cofan and D. Cinghita, *Electroanalysis*, 2008, **20**, 1346–1353.

84   K. Tyszczuk-Rotko, I. Bęczkowska, M. Wójciak-Kosior and I. Sowa, *Talanta*, 129AD, **2014**, 384–391.

85   O.-W. Lau, S.-F. Luk and Y.-M. Cheung, *Analyst*, 1989, **114**, 1047–1051.

86   G. Rocchitta, A. Spanu, S. Babudieri, G. Latte, G. Madeddu, G. Galleri, S. Nuvoli, P. Bagella, M. Demartis, V. Fiore, R. Manetti and P. Serra, *Sensors*, 2016, **16**, 780–801.

87   I. Navarro, D. Gonzalez-Arjona, E. Roldan and M. Rueda, *J. Pharm. Biomed. Anal.*, 1988, **6**, 969–976.

88   Ľ. Švorc, J. Sochr, M. Rievaj and D. Bustin, *Sens. Electroanal.*, 2012, **7**, 393–408.

89   A. Babaei, M. Afrasiabi, S. Mirzakhani and A. Taheri, *J. Braz. Chem. Soc.*, 2011, **22**, 344–351.

90   A. Santos, F. Vicentini, P. Deroco, R. Rocha-Filho and O. Fatibello-Filho, *J. Braz. Chem. Soc.*, 2015, **26**, 2159–2168.

91   A. Moghaddam, A. Mohammadi, S. Mohammadi, D. Rayeji, R. Dinarvand, M. Baghi and R. Walker, *Microchim. Acta*, 2010, **171**, 377–384.

92   M. Afrasiabi, S. Kianipour, A. Babaei, A. Nasimi and M. Shabanian, *J. Saudi Chem. Soc.*, 2016, **20**, S480–S487.

93   Y. Liu, Y. Zhao, B. Sun and C. Chen, *Acc. Chem. Res*, 2013, **46**, 702–713.

94   A. Rao, E. Richter, S. Bandow, B. Chase, P. Eklund, K. Williams, S. Fang, K. Subbaswamy, M. Menon, A. Thess, R. Smalley, G. Dresselhaus and M. Dresselhaus, *Science (80-.).*, 1996, **275**, 187–191.

95   J. Doweiko and D. Nompleggi, *J. Parenter. Enter. Nutr.*, 1991, **15**, 476–483.

96   T. Peters, *All about Albumin: Biochemistry, Genetics and Medical Applications*, Academic Press, London, 1st edn., 1995.

97   J. Nicholson, M. Wolmarans and G. Park, *Br. J. Anaesth.*, 2000, **85**, 599–610.

98   P. Daneshgar, A. Moosavi-Movahedi, P. Norouzi, M. Ganjali, A. Madadkar-Sobhani and A. Saboury, *Int. J. Biol. Macromol.*, 2009, **45**, 129–134.

99   13/417,283, 2013, 1–6.

100   A. Bard and L. Faulkner, *Electrochemical Methods Fundamentals and Applications*, John Wiley & Sons, inc., New York, 2nd edn., 2001.

101   A. Fisher, *Electrode Dynamics*, Oxford University Press, Oxford, 1st edn., 2009.

102   S. Arvydas, in *Electrochemistry of Metal Complexes*, eds. F. Endres, D. MacFarlane and A. Abbott, Wiley-VCH, Weinheim, 1st edn., 2015, pp. 33–50.

103   G. Mabbott, *J. Chem. Educ.*, 1983, **60**, 697–702.

104   M. Lambrechts and W. Sansen, in *Biosensors: Microelectrochemical Devices*, eds. M. Lambrechts and W. Sansen, Taylor & Francis Group, Abingdon, Oxon, 1st edn., 1992, pp. 20–75.

105   K. Samuel, in *Handbook of Instrumental Techniques for Analytical Chemistry*, ed. F. Settle, Prentice Hall, Inc., New Jersey, 1st edn., 1997, pp. 709–725.

106   S. Rifkin and D. Evans, *Anal. Chem.*, 1976, **48**, 2174–2179.

107   W. Carmody, *J. Chem. Educ.*, 1961, **38**, 559–560.

108   Z. J. Ayres, A. J. Borrill, J. C. Newland, M. E. Newton and J. V Macpherson, *Anal. Chem.*, 2016, **88**, 974–980.

109   L. Hutton, M. Newton, P. Unwin and J. Macpherson, *J. Anal. Chem.*, 2009, **81**, 1023–1032.

110   L. A. Hutton, J. G. Iacobini, E. Bitziou, R. B. Channon, M. E. Newton and J. V Macpherson, *Anal. Chem.*, 2013, **85**, 7230–7240.

111   A. Shrivastava, *Chronicles Young Sci.*, 2011, **2**, 21–25.

112   A. Fagan-Murphy, F. Watt, K. Morgan and B. Patel, *J. Electroanal. Chem.*, 2012, **684**, 1–5.

113   P. Watson, I. Watson and R. Batt, *Am. J. Clin. Nutr.*, 1980, **33**, 27–29.

114   M. Hernández, N. Russo, M. Panizza, P. Spinelli and D. Fino, *Diam. Relat. Mater.*, 2014, **44**, 109–116.

115   A. Kraft, *Int. J. Electrochem. Sci.*, 2007, **2**, 355–385.

116   T. Goto, T. Yasukawa, K. Kanda, S. Matsui and F. Mizutani, *Anal. Sci.*, 2011, **27**, 91–94.

117   R. Trouillon, D. O'Harea and Y. Einagab, *Phys. Chem. Chem. Phys.*, 2011, **13**, 5422–5429.

118   S. Alwarappan, D. Wong and S. Butcher, *Sensors Actuators B Chem.*, 2007, **128**, 299–305.

119   J. Foord and D. Opperman, *MRS Proc.*, 2006, **956**, 97-103.

120   N. Wangfuengkanagul and O. Chailapakul, *J Pharm Biomed Anal*, 2002, **28**, 841–847.

121   L. Mazaleuskaya, K. Sangkuhl, C. Thorn, G. FitzGerald, R. Altman and T. Klein, *Pharmacogenet Genomics*, 2015, **25**, 416–426.

122   G. Jarad and J. Miner, *Curr Opin Nephrol Hypertens*, 2009, **18**, 226–232.

123   L. G and C. J, *J Pharm Biomed Anal*, 1994, **12**, 1563–1572.

124   A.-O. S, L. W. P. A, M. P, G. J and M. J, *J Pharm Biomed Anal*, 1995, **13**, 1033–1039.

125   T. Gicquel, J. Aubert, S. Lepage, B. Fromenty and I. Morel, *J. Anal. Toxicol.*, 2013, **37**, 110–116.

126   H. Zeng, P. Arumugam and J. Carlisle, *Phys. Status Solidi A Appl. Mater.*, 2014, **211**, 2785–2789.

127   W. Bagnall, J. Kelleher, B. Walker and M. Losowksy, *J. Pharm. Pharmacol.*, 1979, **31**, 157–

160.

128   L. Prescott, *Med Clin North Am*, 1974, **58**, 907–916.

129   R. Heading, J. Nimmo, L. Prescott and P. Tothill, *Br. J. Pharmacol.*, 1973, **47**, 415–421.

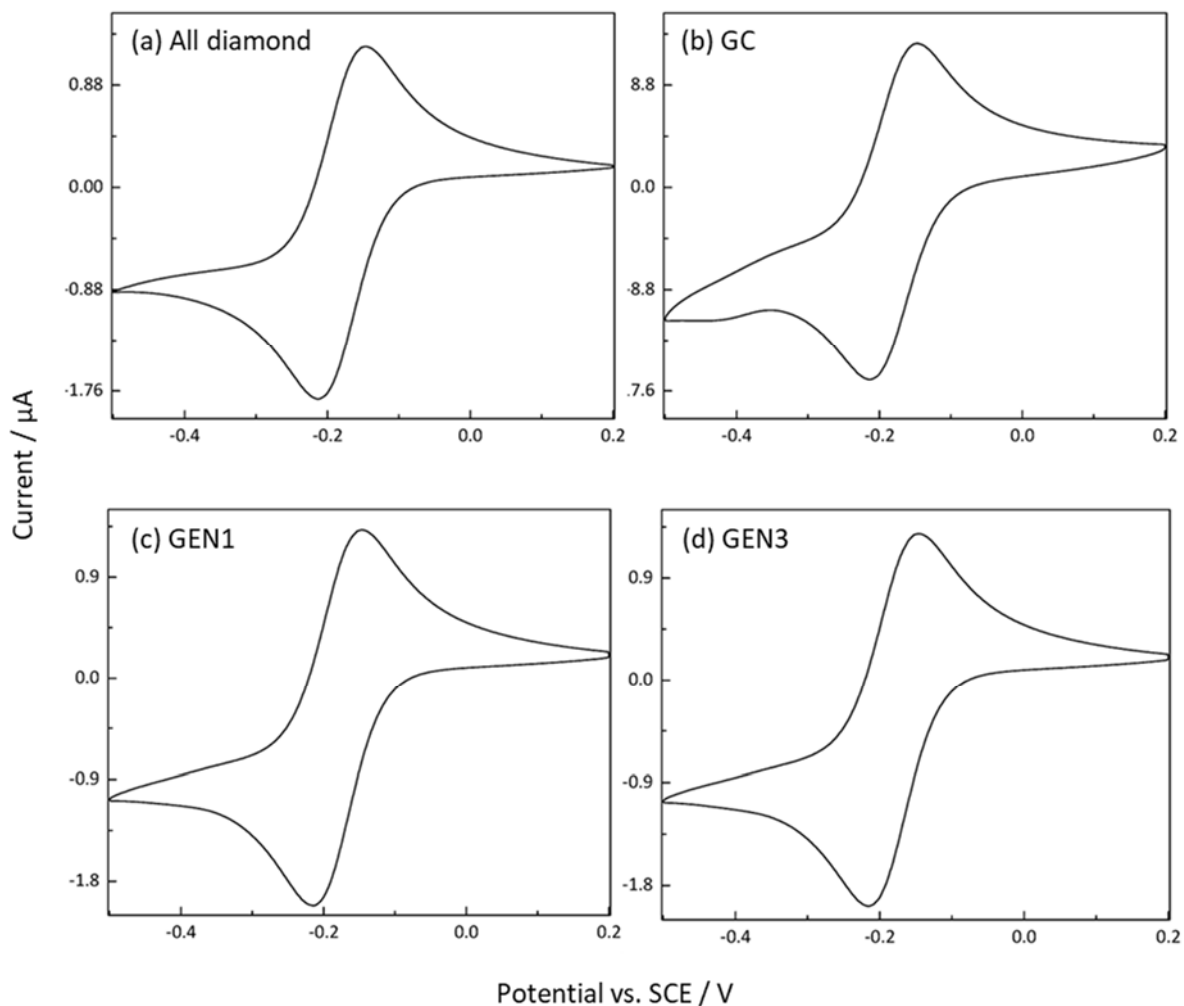# 7. Supplementary Information

7.1 Electrode Characterisation

Figure S1. CV response of 1 mM Ru(NH₃)₆³⁺ in 0.1 M KNO₃ using (a) all diamond, (b) GC, (c) GEN1 and (d) GEN3 electrodes (v = 0.1 V s⁻¹).

Table S1. Electrode areas calculated for each electrode materials from the peak currents in Fig. S1.

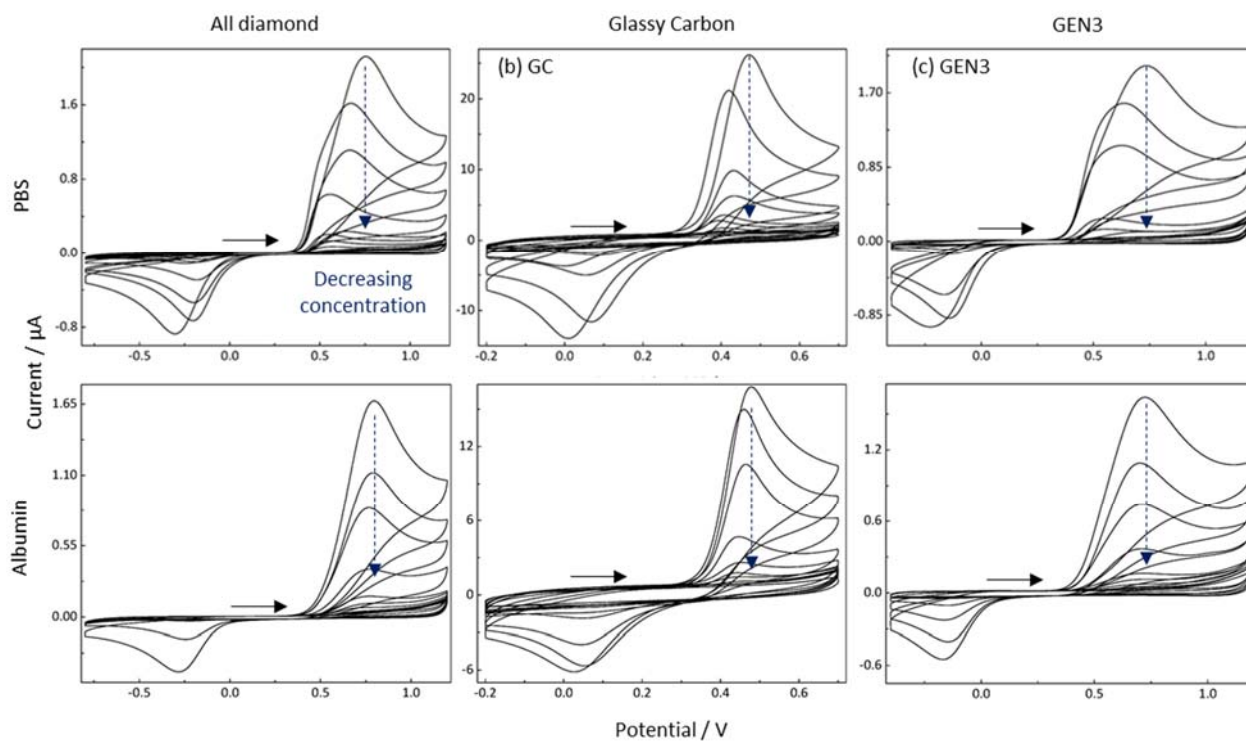| Electrode Material	I_{pc} / μA	Diameter / mm
All diamond	-1.824 x 10-6	0.937
Glassy Carbon	-1.670 x 10-5	2.835
GEN1	-2.008 x 10-6	0.983
GEN3	-1.977 x 10-6	0.975

7.2   Albumin LOD and LOQ CVs

Figure S2. CV response of APAP (ranging from 0.5 µM to 1000 µM) in PBS (pH = 7.4) and 4% albumin using all diamond, GC and GEN3 electrodes (v = 0.1 V s^{-1}).
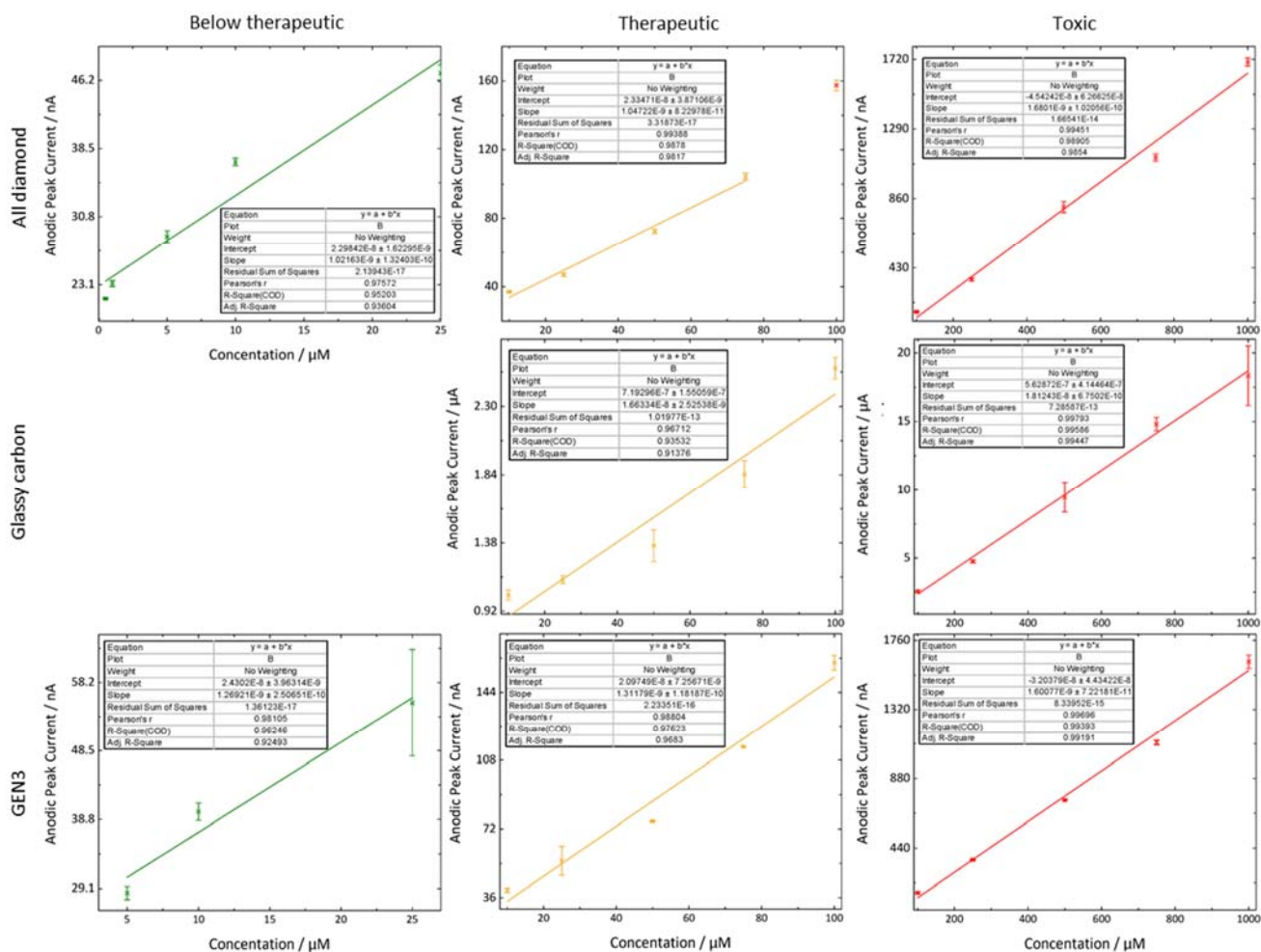
Figure S3. Calibration graphs produced from the peak currents of the CVs taken of PBS (pH = 7.4) (Fig. S2) obtained using all diamond, GC and GEN3 electrodes. The calibration graphs produced cover below therapeutic (green), therapeutic (yellow) and toxic (red) APAP blood concentration ranges. Error bars were produced from the standard deviation of triplicate measurements. A therapeutic concentration calibration graph was not produced as no peaks were visible within the concentration range.

Figure S4. Calibration graphs produced from the LOD CVs taken of 4% BSA (Fig.2) obtained using all diamond, GC and GEN3 electrodes. The calibration graphs produced cover below therapeutic (green), therapeutic (yellow) and toxic (red) APAP blood concentration ranges. Error bars were produced from the standard deviation of triplicate measurements. The current measured at 100 µM in the lethal calibration graph of the all diamond device was excluded from the calibration graph. A therapeutic concentration calibration graph was not produced as no peaks were visible within the concentration range.
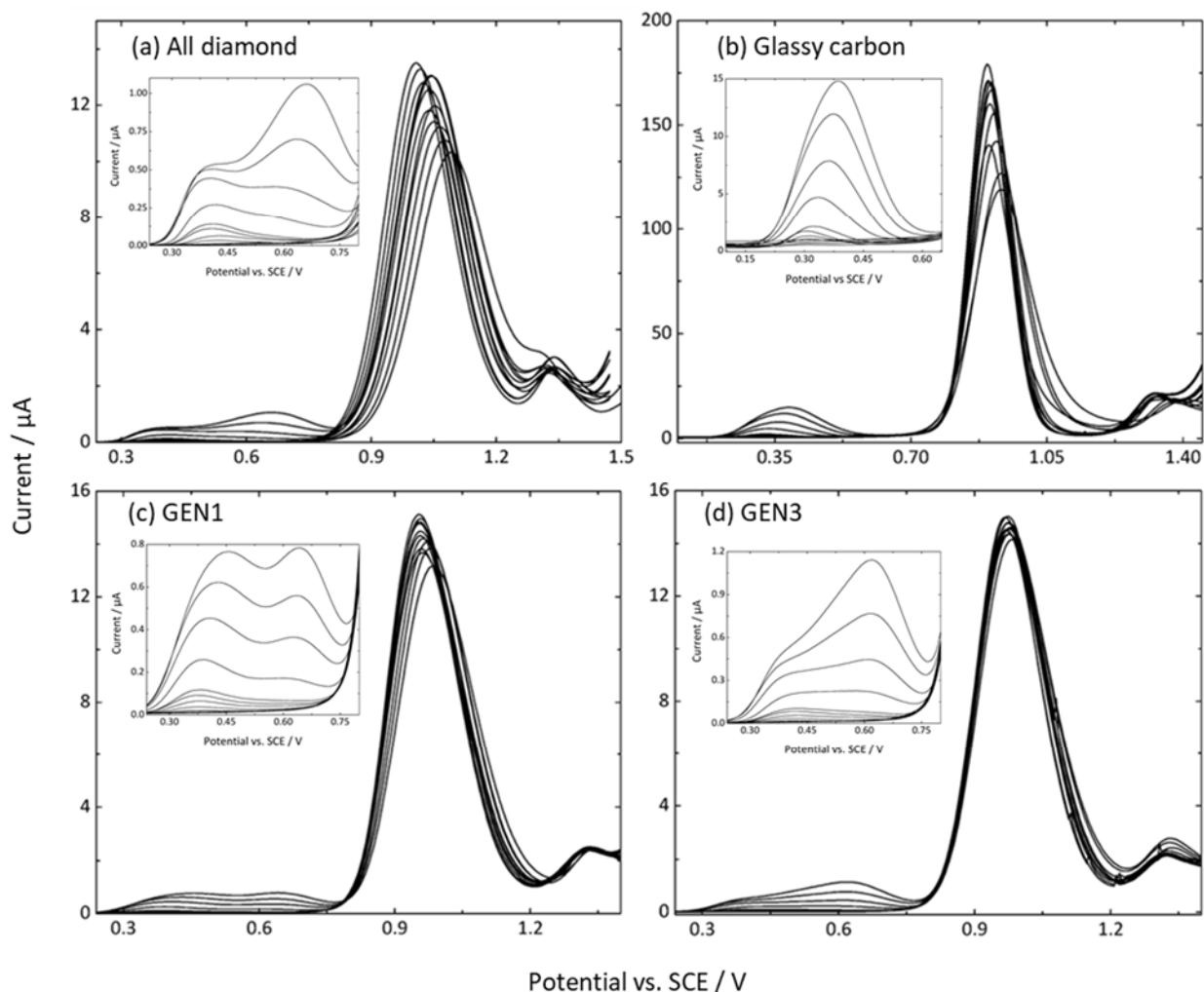
7.3 Synthetic Urine LOD and LOQ DPVs

Figure S5. DPV response of APAP (ranging from 0.5 μM to 1000 μM) in synthetic urine (pH = 6.9) and caffeine (1 mM) using (a) all diamond, (b) GC, (c) GEN1 and (d) GEN3 electrodes. The following operating parameters were utilised: initial potential = 0 V, final potential = 1.475 V, increment potential = 0.004 V, amplitude = 0.1 V, pulse width = 0.2 s, sample width = 0.02 s, pulse period = 0.5 s, quiet time = 2 s, and sensitivity = 1×10^{-5} A/ V. The anodic peak current of the peak at +0.40 V was used to plot calibration graphs.
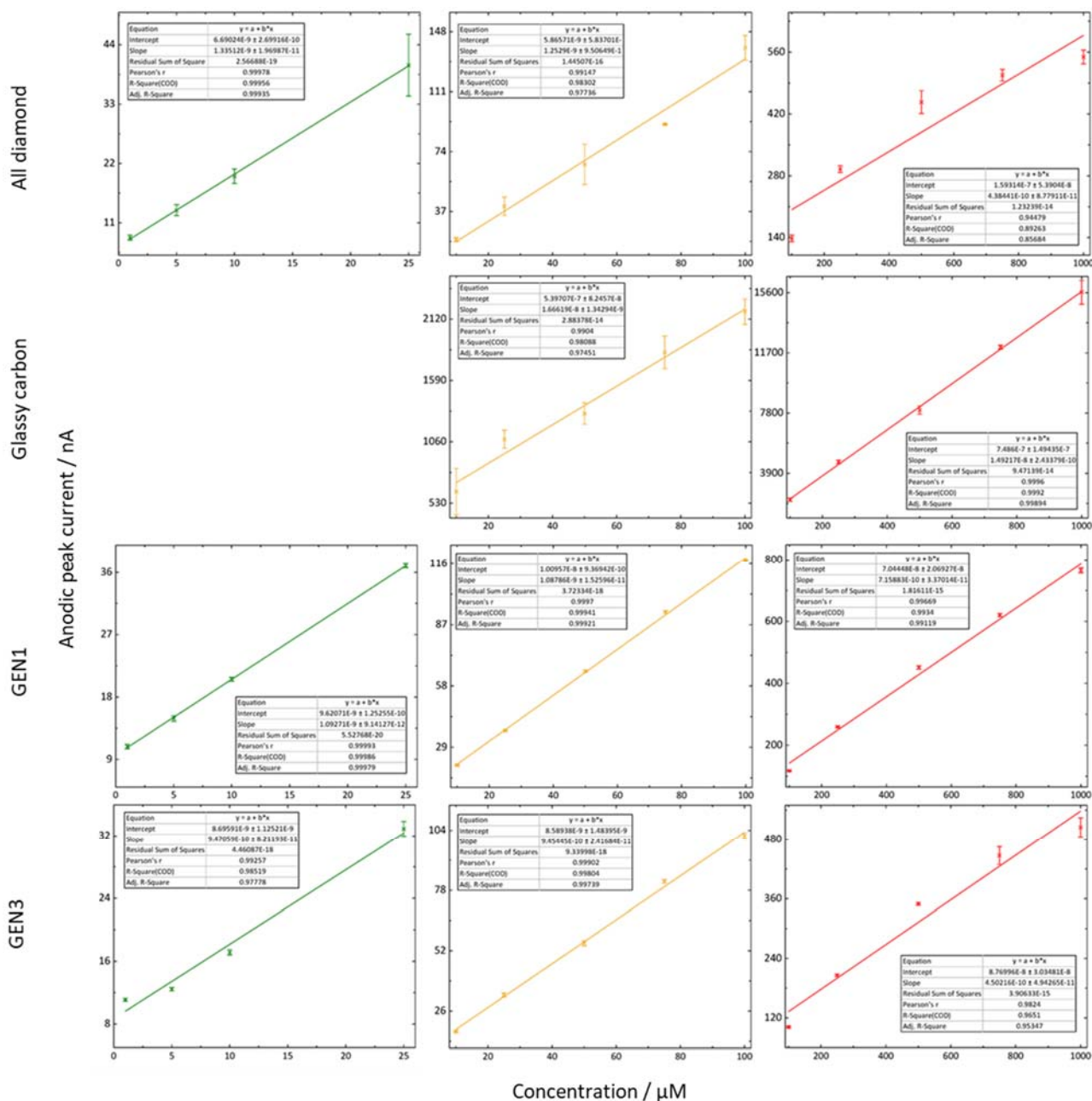
Figure S6. Calibration graphs produced from the DPVs taken of APAP in surine and caffeine (Fig. s5) obtained using all diamond, GC, GEN1 and GEN3 electrodes. The calibration graphs produced cover below therapeutic (green), therapeutic (yellow) and toxic (red) APAP blood concentration ranges. The below therapeutic graph covers the therapeutic range of APAP content in urine. Error bars were produced from the standard deviation of triplicate measurements.
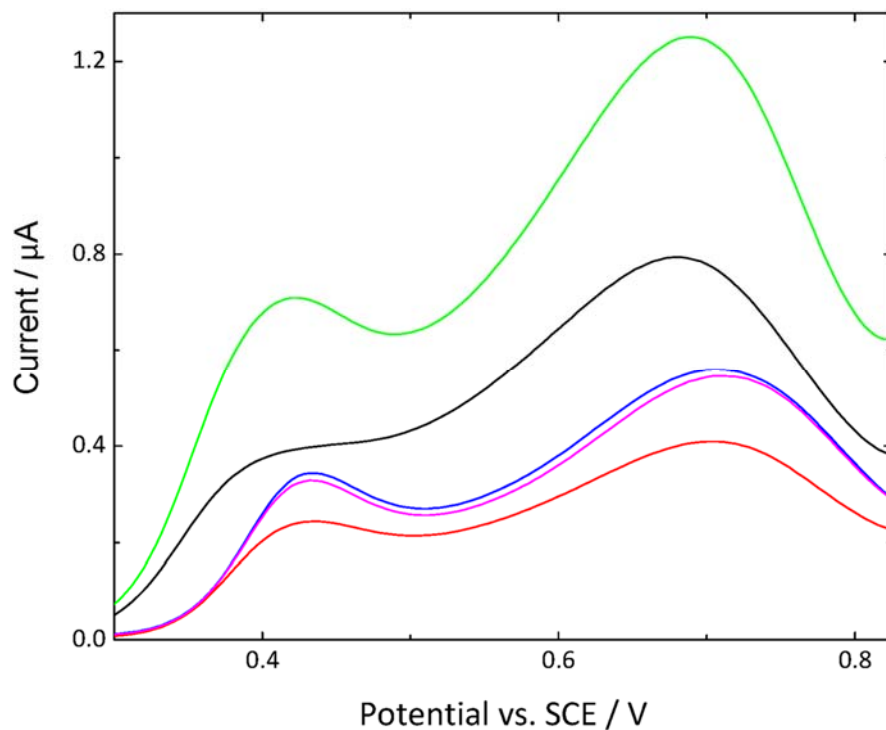
7.4   Optimisation DPV

Figure S7. Optimisation of the DPV method (red line; parameters found in S6), was attempted by changing the amplitude to 0.05 V (red line); amplitude to 0.05 V and pulse width to 0.05 s (blue line); amplitude to 0.05 V, pulse width to 0.05 s, and sampling period to 0.08 s (magenta line), and pulse width to 0.5 s (green line).